6-2009

Communications and Positioning in Wireless Networks

Yao Zhao
Western Michigan University

COMMUNICATIONS AND POSITIONING IN WIRELESS NETWORKS

by

Yao Zhao

A Dissertation
Submitted to the
Faculty of The Graduate College
in partial fulfillment of the
requirements for the
Degree of Doctor of Philosophy
Department of Electrical and Computer Engineering
Advisor: Liang Dong, Ph.D.

Western Michigan University
Kalamazoo, Michigan
June 2009

COMMUNICATIONS AND POSITIONING IN WIRELESS NETWORKS

Yao Zhao, Ph.D.

Western Michigan University, 2009

My doctoral research for the past three years is presented in this report. My research mainly focuses on the communications and positioning for wireless networks and is composed of three parts. First, I explored a new Turbo frequency equalization technique for multiple-input multiple-output (MIMO) wireless communications systems to improve the performance of wireless communications. In the second part of my research, I studied the multiple antenna cooperative communications from the perspective of information theories. The third part of my work is dedicated to extensive research on positioning technology for wireless networks using knowledge of the estimation theory in signal processing.

TABLE OF CONTENTS

Table of Contents—continued

CHAPTER

Table of Contents—continued

LIST OF TABLES

LIST OF FIGURES

List of Figures—continued

CHAPTER 1

INTRODUCTION

The research area of wireless networks contains tons of interesting topics to study. To start with, we decided to study communications of wireless networks and investigate some advanced technologies, such as the Single Carrier, Turbo Equalization, etc. This gave birth to the idea of the chapter 2 " Frequency-Domain Turbo Equalization for Single-Carrier Mobile Broadband Systems", whose abstract is presented below.

Mobile broadband communications, which undergo time-varying radio channels with large multipath delay spread, are investigated in this chapter. Considering that single-carrier (SC) modems with frequency domain equalization have similar performance and complexity as orthogonal frequency-division multiplexing (OFDM), yet less sensitive to radio frequency (RF) impairments, we adopt single-carrier modulation at the transmitter to combat inter-symbol-interference (ISI) resulted from the multipath delay. Space-time block transmission is employed as the transmitting diversity scheme. At the receiver, we propose the Turbo equalization consisting of minimum mean-square error (MMSE) equalization in frequency domain and channel decoding. Moreover, to cope with faster time-varying characteristics of the mobile channel, the data frame can be partitioned into smaller units, or blocks, for space-time block transmission and the linear equalizer. All processed blocks are then combined back to a frame as the input of the channel decoder. Simulation results show good performance of the proposed scheme with feasible computational complexity.

After research on specific wireless communications technologies, we moved on to systematically study the performance of wireless communications from the perspective of information theories and analyze the capacity of cooperative communications where

multiple antennas are adopted at multiple cooperative users. The results are reported in the chapter 3 "Realization and Capacity Analysis of Cooperative Communications based on Multiplexing", whose abstract is presented below.

Cooperative communication (CC) techniques, which form virtual multiple input multiple output (MIMO) systems through cooperation among users, have been prevailing in current academic research. Two scenarios that have been mostly considered are one source to one destination with help from a relay node and two sources to one destination with cooperation among sources, i.e. cooperation for multiple access channels. In either case, single antenna is employed at each node. In this chapter, I propose to realize cooperation based on multiplexing for a broadcast channel where there is one source equipped with multiple antennas and two destinations with single antenna. One of the destinations experiencing better channels helps the other destination under worse channel conditions by serving as a relay. Such a channel is referred to as a multiple input single output (MISO) cooperative broadcast channel (CBC). Further, I consider the capacity analysis for the MISO CBC where additive white Gaussian noise (AWGN) presents (MISO AWGN CBC), which is not easy because MISO AWGN channel, as a vector Gaussian channel, is generally not degraded. I derive an outer bound on the capacity region of MISO AWGN CBC to provide insights into its information transmission limit.

The purpose of research is to solve the problems raised in the real world. Research in previous parts armed us with advanced technologies and theories, and we are ready to apply them for solving some practical problems. We selected to investigate the problems of positioning in wireless networks. We proposed our own positioning algorithms after extensive literature survey and study of existing positioning methods and algorithms. Furthermore, we implemented our algorithm on ZigBee devices for testing in real environments. Details can be found in the chapter 4 "Implementing Indoor Positioning System via ZigBee Devices", whose abstract is presented below.

A wireless indoor positioning system is implemented with the ZigBee technology that has applications in smart office and home, and in industrial automation and

control. We propose an effective cooperative localization algorithm that is tailored to the ZigBee profiles. It combines multidimensional scaling with maximum likelihood estimation, and overcomes their inherent drawbacks. ZigBee devices with chipset reference designs or design-in modules are used for hardware implementation. An indoor positioning testbed is developed to evaluate the algorithm and check the positioning accuracy based on various channel measurements.

The positioning algorithm proposed in the chapter 4 can be improved by using Bayesian estimators instead of classical estimators. The new and better positioning algorithm is proposed and compared with other existing algorithms in the chapter 5 "MMSE Cooperative Positioning in Wireless Networks", whose abstract is presented below.

The Global Positioning System (GPS) is not always available, accurate enough or cost efficient for locating nodes in wireless networks, which motives extensive studies on a variety of none-GPS positioning algorithms. All these algorithms can be classified as non-cooperative methods or cooperative methods. The cooperative methods, though more complicated, achieve better performance since the position estimation for any node is based on information concerning all nodes altogether. In this work, we proposed and derived an minimum mean squared error (MMSE) cooperative positioning method based on the power decays between each pair of wireless nodes. Log-normal power distribution is assumed and verified by the actual field measurements by ZigBee equipments. MMSE positioning based on log-normal power distribution involves complicated multiple integrals, which have no closed form solution. We adopted Simpon quadrature or Monte Carlo numerical methods to obtain the needed integrals. For improved performance, we proposed several variations of our basic MMSE cooperative positioning algorithm. The MMSE positioning algorithm in this work can also be carried out in a non-cooperative way and provides better initial position estimates for some existing iterative positioning approaches. The proposed MMSE cooperative positioning algorithm is optimum in terms of the Root Mean Square Error (RMSE). This is guaranteed by theoretical analysis and is also veri-

fied by the numerical results in comparison with several popular existing cooperative methods.

An iterative and computationally efficient method based on the MMSE positioning algorithm proposed in previous chapter is proposed and compared with other existing algorithms in the chapter 6 "Iterative Cooperative Positioning in Wireless Network", whose abstract is presented below.

The previously proposed MMSE position estimator is a promising cooperative positioning method among all of positioning algorithms due to its excellent accuracy in terms of RMSE. However, direct calculation of the multiple integrals present in MMSE formulas via numerical methods has high computation burden and thus restrict its practical application to a small number of unknown nodes. To overcome this complexity obstacle, we propose an innovative MMSE Adaptive Iterative Cooperative (AIC) method, whose mechanism resembles a turbo engine. This MMSE-AIC positioning method avoids direct calculation of the multiple integrals via adaptive iterative estimation, and its performance is approximately the same as the perfect performance of the exact original MMSE in terms of RMSE. The proposed MMSE-AIC is a practical solution and extends the application of MMSE estimator to large size wireless networks.

CHAPTER 2

FREQUENCY-DOMAIN TURBO EQUALIZATION FOR SINGLE-CARRIER MOBILE BROADBAND SYSTEMS

2.1 Introduction

Single carrier (SC) modulation and orthogonal frequency-division multiplexing (OFDM) are two major techniques to combat the inter-symbol-interference (ISI) characterizing the dispersive channels in wireless broadband systems. Much work has been done to compare these two approaches [1] [2] [3]. Although OFDM has already been applied in many practical applications, SC has been gaining greater popularity due to the disadvantages inherent in OFDM and the fact that when combined with frequency domain equalization, the SC approach delivers performance similar to OFDM, with essentially the same overall complexity [4]. In addition, SC modulation uses a single carrier, instead of the many sub-carriers typically used in OFDM, so the peak-to-average ratio (PAR) of transmitted power for SC-modulated signals is smaller. This means that the power amplifier of an SC transmitter requires a smaller linear range to support a given average power, and thus SC can use cheaper power amplifiers than a comparable OFDM system.

Diversity transmission using Alamouti's space-time block-coding (STBC) scheme [5] has been proposed in several wireless standards due to its many attractive features. It achieves full spatial diversity at full transmission rate for two transmit antennas, without requiring channel state information at the transmitter. And the maximum likelihood decoding for Alamouti's STBC requires only simple linear processing.

Therefore, in this chapter, we consider multi-antenna wireless broadband systems, where STBC with cyclic-prefix (CP) is applied with SC at the transmitter. Convolutional encode is adopted as the forward error control (FEC) scheme.

At the receiver, we propose a frequency domain Turbo equalization to detect the transmitted information bit stream. The Turbo equalization, first proposed in [6], borrowed the idea of Turbo code-decoding to detect iteratively the original information bits impaired by ISI. The outer code is usually a convolutional code and the ISI channel, equivalent to the inner code, is considered as a rate one convolutional code in real Galois field [7]. The extrinsic information transfer (EXIT) chart is used as a theoretical tool for performance analysis. It is well demonstrated that such an iterative scheme provides a significant performance gain. In this chapter, our proposed Turbo equalizer is composed of a linear minimum mean-square error (MMSE) in frequency domain and a soft-input-soft-output (SISO) decoder. The received data are converted to frequency domain and partitioned into blocks before fed into the linear MMSE, and the original information bits are decoded in an iterative and feedback way.

MMSE space-frequency equalization for SC multiple-input multiple-output (MIMO) systems over frequency-selective channels is proposed in [8], but it can not be implemented iteratively to form Turbo equalization because it assumes fixed statistics about the transmitted signals. Borrowing ideas from MMSE using *A priori* information [9], we proposed frequency-domain MMSE equalizer based on dynamic *a priori* information to cooperate with the SISO outer decoder to realize the Turbo equalizer. *a priori* information is updated at each iteration by the SISO decoder. Perfect channel state information (CSI) is assumed to be known to the receiver.

Bit-error-rate (BER) curves and EXIT charts obtained through simulations show excellent performance and validate our proposed approach.

The remaining of this chapter is organized as follows. In section 2.2, the system model is described mathematically. Then, the algorithms of frequency domain Turbo equalizer at the receiver, which is the focus of this chapter is stated in details in the

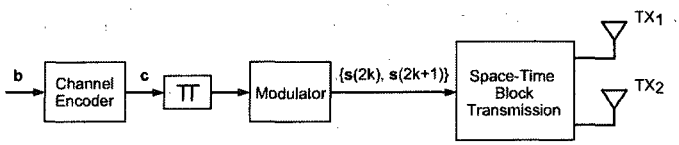

Figure 2.1. Transmitter baseband block diagram: channel encoding and space-time block transmission.

section 2.3. Numerical results through simulations are presented in the section 2.4. Conclusions are made in the section 2.5.

2.2 System Model

2.2.1 Space-Time Transmission

Figure 2.1 depicts the block diagram of a wireless transmitter with two antennas. The binary bit stream **b** is encoded using a convolutional code and becomes code data **c**, which are then randomly interleaved in order that the influence of error bursts is reduced at the input of the channel decoder at the receiver. The interleaved code bits are then modulated and mapped to symbols **s** to compose a frame of length M, which is then partitioned into smaller units, termed *blocks*, of length N. A pair of two blocks are transmitted through the two antennas using Alamouti's space-time block transmission scheme. Suppose P_s pairs (two blocks) are obtained from partition, then we have $N = M/(2P_s)$. N can be set to be larger or smaller to be adaptive to slower or faster time-varying mobile channels. The transmission uses a single carrier frequency. In this chapter, we assume a coherent symbol-spaced receiver frontend with perfect symbol timing and describe the system with an equivalent discrete-time baseband model.

Let $\mathbf{s}(2k)$ and $\mathbf{s}(2k+1)$ denote two consecutive symbol blocks as

$$\begin{aligned} \mathbf{s}(2k) &= [s(2kN), s(2kN+1), \ldots, \\ &\quad s(2kN+N-1)]^T \qquad (2.1) \\ \mathbf{s}(2k+1) &= [s((2k+1)N), s((2k+1)N+1), \ldots, \\ &\quad s((2k+1)N+N-1)]^T \qquad (2.2) \end{aligned}$$

These two symbol blocks are transmitted through the two antennas in the following form analogous to the Alamouti space-time code,

$$\begin{bmatrix} \mathbf{s}(2k) & -\mathbf{P}\mathbf{s}^*(2k+1) \\ \mathbf{s}(2k+1) & \mathbf{P}\mathbf{s}^*(2k) \end{bmatrix} \quad \begin{matrix} \rightarrow \text{ time} \\ \downarrow \text{ space} \end{matrix} \qquad (2.3)$$

where $\mathbf{P}$ is a permutation matrix that is drawn from a set of permutation matrices $\{\mathbf{P}^{(n)}\}_{n=0}^{N-1}$. Each $\mathbf{P}^{(n)}$ performs a reverse cyclic shift, such that when it is applied to a $N \times 1$ vector $\mathbf{s} = [s(0), \ldots, s(N-1)]^T$, the p-th entry of $\mathbf{P}^{(n)}\mathbf{s}$ is $s((N-p+n) \bmod N)$. For example

$$\mathbf{P}^{(0)}\mathbf{s} = [s(N-1), s(N-2), \ldots, s(0)]^T \qquad (2.4)$$

$$\mathbf{P}^{(1)}\mathbf{s} = [s(0), s(N-1), s(N-2), \ldots, s(1)]^T \qquad (2.5)$$

Suppose that the transmit filter, the broadband channel with inter-symbol interference, and the receive filter can be represented by a discrete-time linear filter with finite-length impulse response (FIR) of length L. The FIR filter can be determined by the sequence $\mathbf{h}_\mu = [h_\mu(0), \ldots, h_\mu(L-1)]^T$, where $\mu = 1, 2$ indicates the transmit antenna. For multiple transmitter-receiver antenna pairs with different channel memory, L is the longest filter length. As shown in Figure 2.2, a cyclic prefix (CP) of length L is added to each transmitted block. Therefore, the inter-block interference can be eliminated by removing the CP at the receiver.

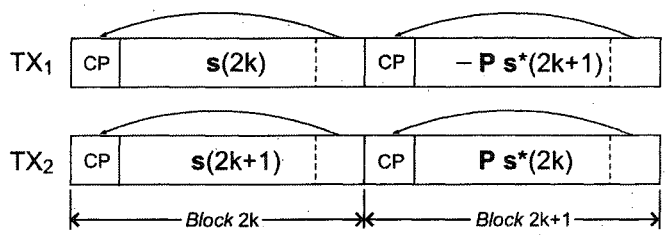

Figure 2.2. Transmitted sequence through two antennas.

2.2.2 Channel Modeling

When the receiver synchronizes to the symbol blocks, the received data in two consecutive blocks are given by

$$\begin{aligned} \mathbf{x}(2k) &= \mathbf{H}_1^{(2k)}\mathbf{s}(2k) + \mathbf{H}_2^{(2k)}\mathbf{s}(2k+1) \\ &\quad +\mathbf{n}(2k) \qquad (2.6) \\ \mathbf{x}(2k+1) &= -\mathbf{H}_1^{(2k+1)}\mathbf{P}\mathbf{s}^*(2k+1) \\ &\quad +\mathbf{H}_2^{(2k+1)}\mathbf{P}\mathbf{s}^*(2k) + \mathbf{n}(2k+1) \qquad (2.7) \end{aligned}$$

where $\mathbf{n}$ is the zero-mean Gaussian noise vector with covariance matrix $\sigma_n^2\mathbf{I}$. It is assumed that the channel is block-invariant, which means the channel stays constant within the transmission of a block. With the removal of CP at the receiver, the channel $\mathbf{H}_\mu^{(j)}$,where $j = 2k, 2k+1$ denotes the j-th symbol block, can be represented by an $N \times N$ circulant matrix as

$$\mathbf{H}_\mu^{(j)} = \begin{bmatrix} h_\mu^{(j)}(0) & 0 & \cdots & h_\mu^{(j)}(1) \\ h_\mu^{(j)}(1) & h_\mu^{(j)}(0) & \cdots & h_\mu^{(j)}(2) \\ \vdots & \vdots & \ddots & \vdots \\ h_\mu^{(j)}(L-2) & h_\mu^{(j)}(L-3) & \cdots & h_\mu^{(j)}(L-1) \\ h_\mu^{(j)}(L-1) & h_\mu^{(j)}(L-2) & \cdots & 0 \\ 0 & h_\mu^{(j)}(L-1) & \cdots & 0 \\ 0 & 0 & \cdots & 0 \\ \vdots & \vdots & \ddots & \vdots \\ 0 & 0 & \cdots & 0 \\ 0 & 0 & \cdots & h_\mu^{(j)}(0) \end{bmatrix} \qquad (2.8)$$

Hence, $\mathbf{H}_{\mu}^{(j)}$ has an eigen-decomposition as

$$\mathbf{H}_{\mu}^{(j)} = \mathbf{F}^{H}\mathbf{\Lambda}_{\mu}^{(j)}\mathbf{F} \tag{2.9}$$

where $\mathbf{F}$ is the orthonormal discrete Fourier transform (DFT) matrix whose $(k,l)-$th entry is $\mathbf{F}_{k,l} = \frac{1}{\sqrt{N}}e^{-j(2\pi/N)kl}$ $(k,l = 0,\ldots,N-1)$. $\mathbf{\Lambda}_{\mu}^{(j)}$ is a diagonal matrix whose $(k,k)-$th entry is given by the k-th DFT coefficient of the first column of $\mathbf{H}_{\mu}^{(j)}$. In addition, the circulant matrix has the following property when operating with the permutation matrix $\mathbf{P}$ [10].

$$\mathbf{P}\mathbf{H}_{\mu}^{(j)*}\mathbf{P} = \mathbf{H}_{\mu}^{(j)H} \tag{2.10}$$

As depicted in Figure 2.3, the receiver divides the symbol blocks to generate $\mathbf{x}(2k)$ and $\mathbf{P}\mathbf{x}^{*}(2k+1)$, which are then passed through FFT modules to be converted to the frequency domain. The resulted outputs are given by

$$\underbrace{\begin{bmatrix} \mathbf{F}\mathbf{x}(2k) \\ \mathbf{F}\mathbf{P}\mathbf{x}^{*}(2k+1) \end{bmatrix}}_{\mathbf{X}(2k)} = \underbrace{\begin{bmatrix} \mathbf{\Lambda}_{1}^{(2k)} & \mathbf{\Lambda}_{2}^{(2k)} \\ \mathbf{\Lambda}_{2}^{(2k+1)*} & -\mathbf{\Lambda}_{1}^{(2k+1)*} \end{bmatrix}}_{\mathbf{\Lambda}^{(2k)}}$$

$$\begin{bmatrix} \mathbf{S}(2k) \\ \mathbf{S}(2k+1) \end{bmatrix} + \underbrace{\begin{bmatrix} \mathbf{F}\mathbf{n}(2k) \\ \mathbf{F}\mathbf{P}\mathbf{n}^{*}(2k+1) \end{bmatrix}}_{\mathbf{W}(2k)} \tag{2.11}$$

where $\mathbf{S}(j) = \mathbf{F}\mathbf{s}(j)$, $j = 2k, 2k+1$. The filtered noise $\mathbf{W}(2k)$ remains white with the same covariance matrix $\sigma_n^2\mathbf{I}$.

The output of the space-time combiner is further fed into a frequency-domain minimum mean square error (MMSE) equalizer to obtain the frequency domain estimates $\hat{\mathbf{S}}(2k)$ and $\hat{\mathbf{S}}(2k+1)$, which are brought back to the time domain via IFFT modules. Finally, the code bits are detected and decoded to the information bits. The details will be explained in the next section.

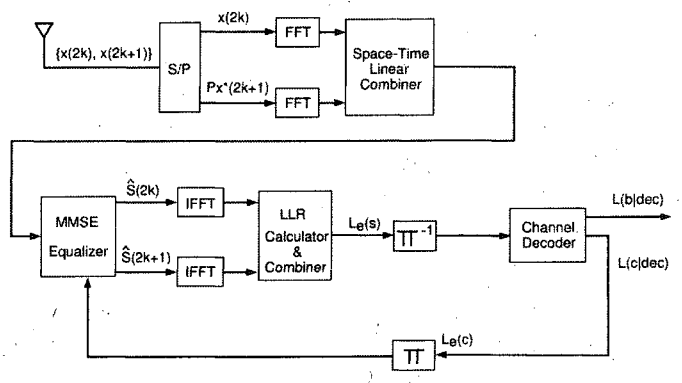

Figure 2.3. Receiver baseband block diagram: space-time combining and Turbo equalization.

2.3 Frequency-Domain Turbo Equalization

2.3.1 Receiver Structure

As shown in Figure 2.3, the receiver consists of a space-time linear combiner, followed by the Turbo equalizer. The Turbo equalizer has two stages: the frequency-domain linear MMSE equalizer and the SISO channel decoder. The two stages are separated by a deinterleaver (a block labeled "π^{-1}") and an interleaver (a block labeled "π"). The *a priori* log-likelihood ratio (LLR) of the symbol bit is fed back to the MMSE equalizer, and the equalizer outputs the *a posteriori* LLR of the symbol bit. For simplicity, the block index (2k) is dropped from now on, i.e. $\mathbf{X} = \mathbf{X}(2k), \mathbf{\Lambda} = \mathbf{\Lambda}^{(2k)}, \mathbf{W} = \mathbf{W}(2k)$. Also, let $\mathbf{S} = \begin{bmatrix} \mathbf{S}(2k) \\ \mathbf{S}(2k+1) \end{bmatrix}$, thus

$$\mathbf{S} = \begin{bmatrix} \mathbf{F} & \mathbf{0} \\ \mathbf{0} & \mathbf{F} \end{bmatrix} \begin{bmatrix} \mathbf{s}(2k) \\ \mathbf{s}(2k+1) \end{bmatrix} = \tilde{\mathbf{F}}\mathbf{s} \tag{2.12}$$

Then, Eq. (2.11) can be rewritten as

$$\mathbf{X} = \mathbf{\Lambda}\mathbf{S} + \mathbf{W} \tag{2.13}$$

BPSK is considered in this chapter. Therefore, the *a priori* LLR is given by

$$L(s(i)) = \ln \frac{P[s(i) = +1]}{P[s(i) = -1]} \tag{2.14}$$

The *a posteriori* LLR is given by

$$L(s(i)|\mathbf{X}) = \ln \frac{p[s(i) = +1|\mathbf{X}]}{p[s(i) = -1|\mathbf{X}]} \tag{2.15}$$

Using Bayes' rule, it can be written as

$$L(s(i)|\mathbf{X}) = \underbrace{\ln \frac{p[\mathbf{X}|s(i) = +1]}{p[\mathbf{X}|s(i) = -1]}}_{L_e(s(i))} + \underbrace{\ln \frac{P[s(i) = +1]}{P[s(i) = -1]}}_{L(s(i))} \tag{2.16}$$

where $L_e(s(i))$ is the extrinsic information. The extrinsic information of all blocks of length N at the output of the MMSE equalizers is calculated and combined back into a frame of length M before being deinterleaved to generate the *a priori* LLR of the code bit for the channel decoder. The decoder outputs an update of the LLR of the code bit and the information bit. The extrinsic information of the code bits based on the code constraints is interleaved and fed back to the corresponding linear MMSE equalizer as the priori information in the next iteration. The *a posteriori* LLR of the information bit is used to make hard decision at the last iteration. Note that the extrinsic information from the MMSE equalizers and from the decoder are statistically independent at the first iteration, but become more and more correlated in the subsequent iterations. Therefore, the improvement through iteration will diminish.

2.3.2 Frequency-Domain Linear MMSE Equalizer

It is assumed that perfect channel estimation is available at the receiver, or in another word, the exact channel matrix is known to the receiver. Then, according to the well-known MMSE formula, the frequency domain estimation $\hat{\mathbf{S}}$ at the output of MMSE equalizer can be obtained as

$$\begin{aligned} \hat{\mathbf{S}} &= [\mathbf{C}_{\mathbf{XX}}^{-1}\mathbf{C}_{\mathbf{XS}}]^H(\mathbf{X} - E(\mathbf{X})) + E(\mathbf{S}) \\ &= [(\mathbf{\Lambda} C_{\mathbf{SS}} \mathbf{\Lambda}^H + \sigma_n^2 \mathbf{I})^{-1} \mathbf{\Lambda} C_{\mathbf{SS}}]^H(\mathbf{X} - \mathbf{\Lambda} E(\mathbf{S})) \\ &\quad + E(\mathbf{S}) \end{aligned} \tag{2.17}$$

where $\mathbf{C_{XX}}, \mathbf{C_{XS}}$ and $\mathbf{C_{SS}}$ are covariance matrices, defined as $\mathbf{C_{x,y}} \equiv Cov(\mathbf{x}, \mathbf{y}) = E(\mathbf{x}\mathbf{y}^H) - E(\mathbf{x})E(\mathbf{y}^H)$. According to Eq. (2.12), $E(\mathbf{S}) = \tilde{\mathbf{F}}E(\mathbf{s})$ with the i-th element $E(s(i))$ depending on the *a priori* LLR $L(s(i))$ as

$$\begin{aligned} E(s(i)) &= \sum_{k\in\{+1,-1\}} k \cdot P[s(i) = k] \\ &= \tanh\left(\frac{1}{2}\ln\frac{P[s(i)=+1]}{P[s(i)=-1]}\right) \\ &= \tanh\left(\frac{L(s_i)}{2}\right) \end{aligned} \tag{2.18}$$

Due to the the independence of the interleaved symbols $\{s(i)\}$ and with the BPSK assumption, the covariance matrix $C_{\mathbf{SS}}$ can be calculated as

$$\begin{aligned} \mathbf{C_{SS}} &= \tilde{\mathbf{F}} C_{\mathbf{ss}} \tilde{\mathbf{F}}^H \\ &= \tilde{\mathbf{F}} diag\left((1 - |E(\mathbf{s})|^2)\right) \tilde{\mathbf{F}}^H \end{aligned} \tag{2.19}$$

where the i-th element of $|E(\mathbf{s})|^2$ is $|E(s(i))|^2$, calculated as shown in Eq. (2.18). The *a priori* LLR $L(s(i))$ is updated in each iteration, so the MMSE estimator must be recomputed for each iteration.

Once the symbol values in the frequency domain are estimated, the time-domain values can be obtained by performing the inverse DFT as

$$\hat{\mathbf{s}} = \tilde{\mathbf{F}}^H \hat{\mathbf{S}} \tag{2.20}$$

At the first Turbo iteration, it is assumed that $s(i)$ is equally likely $+1$ or -1 which yields $E(\mathbf{S}) = E(\mathbf{s}) = 0$ and $\mathbf{C_{SS}} = \mathbf{I}$. The MMSE estimator as shown in Eq. (2.17) can be simplified as

$$\hat{\mathbf{S}} = [(\mathbf{\Lambda}\mathbf{\Lambda}^H + \sigma_n^2\mathbf{I})^{-1}\mathbf{\Lambda}]^H\mathbf{X} \tag{2.21}$$

Assume that the probability density function $p[\hat{s}(i)|s(i) = k], k = \pm 1$ is Gaussian with mean $\mu_{i,k} = E\{\hat{s}(i)|s(i) = k\}$ and variance $\sigma_{i,k}^2 = \text{cov}\{\hat{s}(i), \hat{s}(i)|s(i) = k\}$. The *a*

posteriori LLR $L(s(i)|\hat{s}(i))$, which is an approximation of $L(s(i)|\mathbf{X})$, can be expressed as

$$L(s(i)|\hat{s}(i)) = \underbrace{\ln \frac{p[\hat{s}(i)|s(i)=+1]}{p[\hat{s}(i)|s(i)=-1]}}_{L_e(s(i))} + \underbrace{\ln \frac{P[s(i)=+1]}{P[s(i)=-1]}}_{L(s(i))} \tag{2.22}$$

The extrinsic information $L_e(s(i))$ can be calculated as

$$\begin{aligned} L_e(s(i)) &= \ln \frac{\exp(-|\hat{s}(i)-\mu_{i,+1}|^2/\sigma_{i,+1}^2)}{\exp(-|\hat{s}(i)-\mu_{i,-1}|^2/\sigma_{i,-1}^2)} \\ &= \frac{|\hat{s}(i)-\mu_{i,-1}|^2}{\sigma_{i,-1}^2} - \frac{|\hat{s}(i)-\mu_{i,+1}|^2}{\sigma_{i,+1}^2} \end{aligned} \tag{2.23}$$

Let $\mathbf{A} = [(\mathbf{\Lambda} C_{\mathbf{SS}} \mathbf{\Lambda}^H + \sigma_n^2 \mathbf{I})^{-1} \mathbf{\Lambda} C_{\mathbf{SS}}]^H$. From (2.17) and (2.20), we have

$$\hat{s}(i) = \mathbf{u}_i \tilde{\mathbf{F}}^H \left(\mathbf{A}(\mathbf{\Lambda S} - \mathbf{\Lambda} E(\mathbf{S}) + \mathbf{W}) + E(\mathbf{S})\right) \tag{2.24}$$

where $\mathbf{u}_i = [0, \ldots, 0, \underbrace{1}_{i^{th}}, 0, \ldots, 0]$. Therefore, it can be derived that

$$\mu_{i,k} = \mathbf{u}_i (\tilde{\mathbf{F}}^H \mathbf{A} \mathbf{\Lambda} \tilde{\mathbf{F}} \mathbf{d}^{(i,k)} + E(\mathbf{s})) \tag{2.25}$$

$$\sigma_{i,k}^2 = \mathbf{u}_i \left(\tilde{\mathbf{F}}^H \mathbf{A} \left(\mathbf{\Lambda} \tilde{\mathbf{F}} \mathbf{C}_{\mathbf{ss}|s(i)=k} \tilde{\mathbf{F}}^H \mathbf{\Lambda}^H + {\sigma_n}^2 \mathbf{I}\right) \mathbf{A}^H \tilde{\mathbf{F}}\right) {\mathbf{u}_i}^H \tag{2.26}$$

where

$$\mathbf{d}^{(i,k)} = [0, \ldots, 0, \underbrace{k - E(s(i))}_{i^{th}}, 0, \ldots, 0]^T$$

and

$$\begin{aligned} \mathbf{C}_{\mathbf{ss}|s(i)=k} &= Cov(\mathbf{s}, \mathbf{s}|s(i)=k) \\ &= \mathbf{C}_{\mathbf{ss}} + diag(0, \ldots, 0, \underbrace{2E(s(i))(E(s(i)) - k)}_{i^{th}} \\ &\quad , 0, \ldots, 0). \end{aligned}$$

At the first Turbo iteration, Eq. (2.25) and (2.26) are simplified as

$$\mu_{i,k} = k \mathbf{u}_i \tilde{\mathbf{F}}^H \mathbf{A} \mathbf{\Lambda} \tilde{\mathbf{F}} {\mathbf{u}_i}^H \tag{2.27}$$

$$\sigma_{i,k}^2 = \mathbf{u}_i \left(\tilde{\mathbf{F}}^H \mathbf{A} \left(\mathbf{\Lambda} \mathbf{\Lambda}^H + {\sigma_n}^2 \mathbf{I}\right) \mathbf{A}^H \tilde{\mathbf{F}}\right) {\mathbf{u}_i}^H \tag{2.28}$$

2.3.3 SISO Channel Decoder

The SISO channel decoder takes the *a priori* LLRs of the code bits as input and outputs the updated LLRs of the code bits $L(c(i)|\text{decoding})$, as well as the LLRs of the information bits $L(b(i)|\text{decoding})$ based upon the code constraints.

We use the log maximum *a posteriori* probability (Log-MAP) decoding algorithm to calculate the *a posteriori* LLRs of the code bits and the information bits. The *a posteriori* LLRs of the code bits can be written as [11]

$$\begin{aligned} L(c(i)|\text{decoding}) &= \ln \frac{P[c(i)=+1]|\text{decoding}]}{P[c(i)=-1]|\text{decoding}]} \\ &= \ln \frac{\sum_{(s',s)\in\Sigma_l^+} p[s_l=s', s_{l+1}=s]}{\sum_{(s',s)\in\Sigma_l^-} p[s_l=s', s_{l+1}=s]} \end{aligned} \tag{2.29}$$

while the *a posteriori* LLRs of the information bits can be written as

$$\begin{aligned} L(b(i)|\text{decoding}) &= \ln \frac{P[b(i)=+1]|\text{decoding}]}{P[b(i)=-1]|\text{decoding}]} \\ &= \ln \frac{\sum_{(s',s)\in U_l^+} p[s_l=s', s_{l+1}=s]}{\sum_{(s',s)\in U_l^-} p[s_l=s', s_{l+1}=s]} \end{aligned} \tag{2.30}$$

where Σ_l^{+1} and Σ_l^{-1} are the sets of all state pairs $s_l = s'$ and $s_{l+1} = s$ that correspond to the code bit $c(i) = +1$ and $c(i) = -1$, respectively. U_l^{+1} and U_l^{-1} are the sets of all state pairs $s_l = s'$ and $s_{l+1} = s$ that correspond to the information bit $b(i) = +1$ and $b(i) = -1$, respectively.

2.4 Numerical Results and Analysis

The performance of our proposed approach is evaluated through simulations. As mentioned in sections 2.2 and 2.3, in order to cope better with the time-varying characteristics of the mobile channel, we partition a frame of encoded date of length M into multiple blocks of length N for the linear equalization and then combine all blocks

to form a frame for the channel decoder. This can also improve the computational efficiency. Specifically in our simulations, $M = 2^{16}$ BPSK modulated symbols are partitioned into $P_s = 256$ pairs of blocks of length $N = 128$. Each of these blocks is processed through the linear MMSE frequency-domain equalizer and the outputs are combined back into a 2^{16} bit frame to be fed into the deinterleaver and the convolutional decoder.

EXIT chart at $E_s/N_0 = -5.2dB$, where E_s is the energy of the transmitted symbol, is plotted in Figure 2.4. It illustrates the mutual information transfer characteristics for the SISO decoder. Figure 2.5 presents the BER performance of each iteration versus E_b/N_0, where E_b is defined as the energy of the information bit. As shown in these figures, the output transfer information increases with each iteration, which indicates more accurate decoding. Correspondingly, BER becomes smaller with more iterations.

Our proposed scheme is designed to deal with ISI caused by frequency selective broadband multi-antenna channel. As for the Alamouti's STBC adopted in this chapter, it's a system of two transmit antennas and one receive, which is labeled as 2×1. To make comparison, the case of frequency-flat or ISI free 2×1 channel and the case of frequency-selective broadband single antenna channel, labeled as 1×1, are also considered. The comparison of BER performance at the fourth iteration is shown in Figure 2.6. It is shown that our proposed algorithm can achieve comparable performance to flat channel, which indicate that the proposed frequency domain Turbo equalization with STBC over single carrier is an effective way to combat ISI. Better performance obtained in 2×1 multi-antenna channel than 1×1 single antenna channel is resulted from the diversity gain brought by STBC.

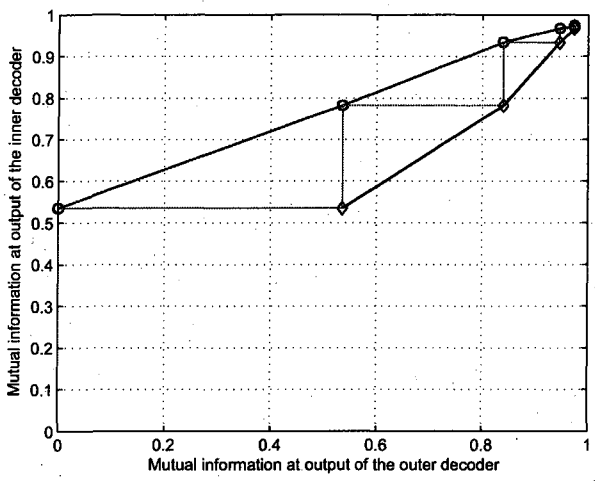

Figure 2.4. EXIT chart , $E_s/N_0 = -5.2dB$.

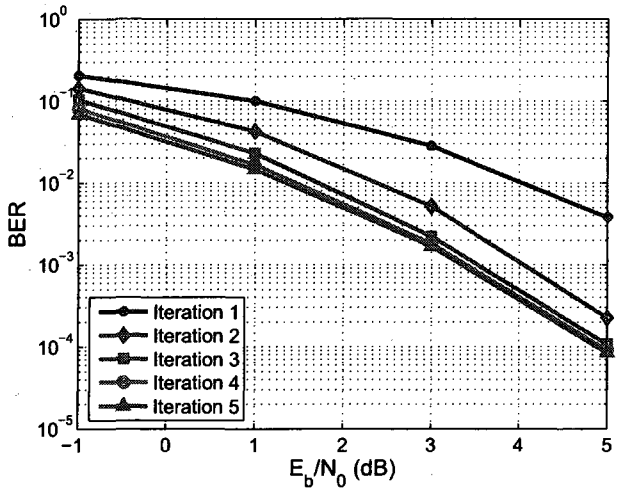

Figure 2.5. BER performance at different iterations.

2.5 Conclusions

A frequency-domain Turbo equalization approach is proposed for space-time block transmission over single-carrier broadband channels. The Turbo equalization is im-

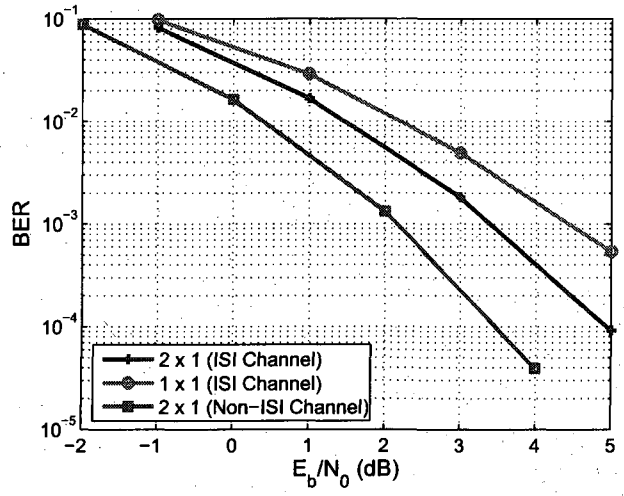

Figure 2.6. BER comparison at the 4^{th} iteration.

plemented through *a priori* information based linear MMSE detector, whose transformation matrix is updated in each iteration according to the updated *a priori* information fedback from the SISO convolutional decoder. Comparison with non-ISI channels through simulations well demonstrates that the proposed frequency domain turbo equalization for single carrier mobile systems is a promising way to combat the distortion caused by ISI channels. Better performance with two transmit antennas than single antenna case is achieved due to the diversity gain resulted from STBC transmission. Furthermore, by partitioning the frame of modulated symbols stream into blocks, the proposed approach is able to deal with faster time-varying mobile channels, because it is only required that the channel should remain constant over the period of a block.

CHAPTER 3

REALIZATION AND CAPACITY ANALYSIS OF COOPERATIVE COMMUNICATIONS BASED ON MULTIPLEXING CHARACTERISTICS

3.1 Introduction

Cooperative communication (CC) receives lots of attentions and efforts in academic research nowadays. While we are working on profound theories of CC, we may not realize that we have already been enjoying this technique in real life. For example, P2P, which provides us with high speed download over Internet, is a typical CC technique, where a user downloads the message from source with the help of other users who send the source message to that user while they are downloading their own messages from the source. The situation gets complicated for wireless CC (WCC), where channel environment is adverse. Over 30 years ago, the relay channel model, which built the foundation for CC, came to people's view through the papers [12,13]. Another milestone paper [14] was written by Thomas M. Cover et al who proved four capacity theorems for the relay channel. The paper [15] provides a comprehensive analysis for relay channel capacity as well as coding schemes which consists of decode-and-forward (DF) and compress-and-forward (CF) coding. The papers [16,17] trigger intensive interests in user cooperation based on relay channel. Among lots of works on user cooperation, the paper [18] presents an overview of CC, a more popular term to refer to user cooperation. An extended work focusing on turbo code to implement CC is studied in the paper [19]. The essence of CC is to form virtual MIMO via cooperation among users with single antenna and exploit the diversity provided by

MIMO to combat the fading channel and increase reliability over communications. Several protocols have been proposed in papers [20,21] to realize a high spatial diversity gain. A complete protocol set is presented in the paper [22], where the authors further propose a new protocol which is best among the existing protocols for the single-relay fading channel. At the same time, some special cases are studied in other papers [23,24]. In the paper [23], a cluster model is studied to achieve higher spatial diversity and the paper [24] investigates asynchronous space-time cooperative communications for sensor and robotic networks. Most models mentioned above can be classified into one of the four types illustrated in Figure 3.1, where (a) is the classical relay model, (b) is the multiple access relay (MAR) system, (c) is the classical CC system and (d) is extended version of CC. "S" ,"R" and "D" stand for the source node, the relay node and the destination node, respectively. Please note that the relay node simply helps the communication between the source and the destination, and does not have its own messages to receive.

As revealed in Figure 3.1, the focus of typical CC systems is on cooperation among multiple sources, or multiple access cooperation. Cooperation can also be implemented in a broadcast channel, where one source communicates with multiple cooperating destinations. Pioneer works on capacity analysis for broadcast channels without user cooperation can be found in works by Thomas M. Cover et al [25–28], which build the foundation for broadcast channel analysis and introduce the degraded Gaussian channel, a concept particular to the broadcast channel. As for broadcast channels with cooperation, intensive study has been done in papers [29,30] by Liang et al, where the authors derive the capacity region of the degraded Gaussian relay broadcast channel and inner/outer bound of the non-degraded Gaussian relay broadcast channel.

All types of existing CC systems discussed before have one thing in common, that is, single antenna is used at all nodes, including source, relay and destination nodes. We can also employ antenna array at some or all of nodes to further improve the

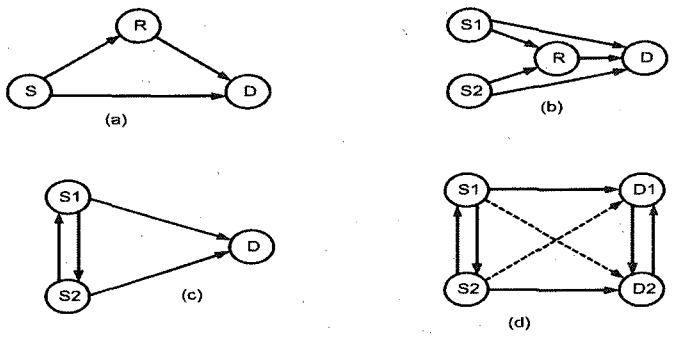

Figure 3.1. Cooperative/relay communication system.

system performance. A relay system with antenna arrays at the source, relay and destination nodes, as shown in Figure 3.2, is proposed and studied in the paper [31].

In this chapter, I consider a broadcast channel with one source and two destinations. The destination under better channel conditions, called the *stronger destination*, serves as a relay for the other destination, called the *weaker destination*. I propose to adopt multiple antennas at the source node. Single antenna is still employed at both destination nodes. Thus multiple input single output (MISO) channel exists between the source and each of the destination. Such a channel is referred to as MISO cooperative broadcast channel (CBC). I further consider MISO CBC corrupted by the additive white Gaussian noise (AWGN), called MISO AWGN CBC, and derive an outer bound on its capacity region.

The capacity analysis of broadcast channels is more complicated than that of the multiple access channel, even without cooperation taken into consideration. Using multiple antennas at the source adds to the difficulty, since MISO AWGN channel, which corresponds to a vector Gaussian channel, is generally non-degraded. A corner stone work for MIMO broadcast capacity analysis is done by Caire-Shamai [32] who investigate the achievable region of MIMO broadcast channel by using the "dirty-paper" precoding technique [33]. An innovative way which considers the duality between uplink and downlink is studied in the papers [34, 35]. As for MISO CBC

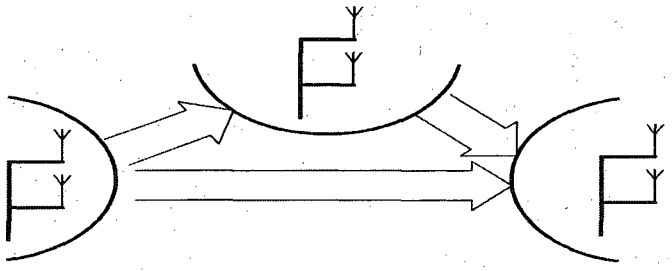

Figure 3.2. MIMO relay system.

studied in this chapter, which is a multi-antenna broadcast channel with cooperation, the capacity analysis has not been done yet. In my work, the outer bound derivation is based on the work on general single antenna relay broadcast channel given in the paper [30].

The remaining of this chapter is organized as follows. In section 3.2, the model for general MISO broadcast cooperative channel is introduced and the mathematical representation of the received signals over AWGN channels is given. The outer bound on the capacity region of MISO AWGN CBC is addressed in section 3.3. The conclusion is made in section 3.4. The proof for the outer bound is outlined in the appendix. Last but not least, my thanks to my wife are presented in acknowledgments section.

Throughout this chapter, for a matrix $\mathbf{A}$, $\mathsf{diag}(\mathbf{A})$ denotes the vector composed of all diagonal elements of $\mathbf{A}$. For a vector $\mathbf{a}$, $\mathsf{diag}(\mathbf{a})$ denotes a diagonal matrix with $\mathbf{a}$ as its diagonal elements. All vectors are column vectors except for the channel fading vectors, which are the row vectors for simpler notations.

3.2 System Model

The model for general MISO CBC, where cooperation is realized between two destinations, is illustrated in Figure 3.3. Without the loss of generality, I assume

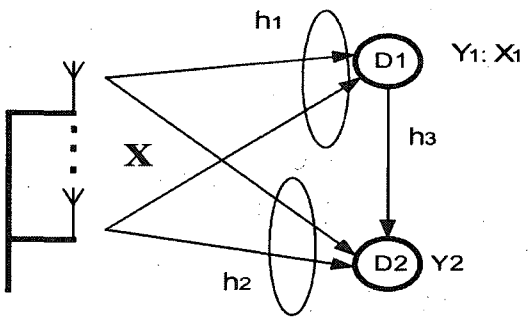

Figure 3.3. MISO CBC.

that the first destination is the stronger destination and thus serves as a relay for the second destination.

For MISO AWGN CBC, the channel coefficients are considered to obtain general results. Suppose there are M antennas at the source. The received signals at two destinations can be presented as

$$\begin{aligned} Y_1 &= \mathbf{h}_1\mathbf{X} + W_1 \\ Y_2 &= \mathbf{h}_2\mathbf{X} + h_3X_1 + W_2 \end{aligned} \tag{3.1}$$

where $\mathbf{X} = [X^{(1)}, X^{(2)}, \cdots, X^{(M)}]^T$ is the transmitted signal vector from the source, X_1 is the relay signal, $\mathbf{h}_i = [h_{i1}, h_{i2}, \cdots, h_{iM}]$ $(i = 1, 2)$ is the channel vector from the source to the i-th destination, and h_3 is the channel from the relay to the second destination. W_i $(i = 1, 2)$ is AWGN with i.i.d. $\mathcal{CN}(0, N_0)$.

For Rayleigh fading, the entries in $\mathbf{h}_1$, $\mathbf{h}_2$ and h_3 are $\mathcal{CN}(0, \mathcal{E}_1)$, $\mathcal{CN}(0, \mathcal{E}_2)$ and $\mathcal{CN}(0, \mathcal{E}_3)$, respectively. As mentioned before, Y_1 is assumed to experience better channels than Y_2, which indicates that $\mathcal{E}_1 > \mathcal{E}_2$. AWGN channels with fixed channel coefficient are equivalent to AWGN channels with fading conditioned on a realization of channel fadings.

The power constraints are imposed and can be presented as $\mathsf{E}(\|\mathbf{X}\|^2) \leq P$ for the total transmission power from all antennas at the source, and $\mathsf{E}(|X_1|^2) \leq P_1$ for the relay. Let $\mathbf{Q_X}$ be the auto correlation matrix for $\mathbf{X}$ and $\mathbf{q}_{\mathbf{X}X_1}$ be the correlation

vector between the source $\mathbf{X}$ and the relay X_1. The power constraint for the source can also be represented as $\mathsf{trace}(\mathbf{Q_X}) \leq P$.

3.3 An Outer Bound on the Capacity Region of MISO AWGN CBC

The information rate of the private messages from the source to the first destination and the second destination are R_1 and R_2, respectively. If common messages are transmitted from the source to both destinations, the rate is R_0. In our work, I do not consider common messages, and thus $R_0 = 0$.

If the channel side information (CSI) is known both to the transmitter and the receiver, the following theorem gives the corresponding outer bound on the capacity region.

Theorem 1. An outer bound on the capacity region of the MISO AWGN CBC, denoted as $C^{(o)}$, conditioned on channel realization $\mathbf{h}_1$, $\mathbf{h}_2$ and h_3, is given by

$$C^{(o)} = \bigcup_{\substack{0\leq\alpha,\varphi\leq 1 \\ \mathsf{trace}(\mathbf{Q_X})\leq P}} \left\{ \begin{array}{ll} R_1 < & \mathcal{C}\left(\frac{\bar{\alpha}\varphi\mathbf{h}_1\mathbf{Q_X}\mathbf{h}_1^H}{\alpha\mathbf{h}_1\mathbf{Q_X}\mathbf{h}_1^H+N_0}\right) \\ R_2 < & \min\left\{ \max_{\substack{\mathbf{q_X}X_1: \\ |\mathbf{q_X}X_1|^2\leq\bar{\varphi}\bar{\alpha}P_1\mathsf{diag}(\mathbf{Q_X})}} \mathcal{C}\left(\frac{\tilde{\mathbf{h}}_2\tilde{\mathbf{Q}}\tilde{\mathbf{h}}_2^H}{N_0}\right), \log\left(\det\left(\mathbf{I}+\frac{1-\bar{\varphi}\bar{\alpha}}{N_0}\tilde{\mathbf{H}}\mathbf{Q_X}\tilde{\mathbf{H}}^H\right)\right)\right. \end{array} \right. \tag{3.2}$$

where $\mathsf{diag}(\mathbf{Q_X})$ is the vector composed of all diagonal elements of $\mathbf{Q_X}$. And $\tilde{\mathbf{h}}_2 = [\ \mathbf{h}_2 \quad h_3\ ]$, $\tilde{\mathbf{H}} = \begin{bmatrix} \mathbf{h}_1 \\ \mathbf{h}_2 \end{bmatrix}$, and $\tilde{\mathbf{Q}} = \begin{bmatrix} \mathbf{Q_X} & \mathbf{q}_{\mathbf{X}X_1} \\ \mathbf{q}_{\mathbf{X}X_1}^H & P_1 \end{bmatrix}$ (the correlation matrix of $[\mathbf{X}^T, X_1]^T$). Also, $\bar{\alpha} = 1-\alpha$, $\bar{\varphi} = 1-\varphi$ and $\mathcal{C}(x) = \log(1+x)$ (for complex signals).

Proof: See Appendix A for the outline of the proof. □

Remark 1: The outer bound for general MISO CBC given in the proof is obtained by a straightforward extension of the outer bound for general single antenna partially cooperative relay broadcast channel (RBC) given in the paper [30] and thus there is no need to prove it again.

Remark 2: While it is straightforward to extend the outer bound for general single antenna partially cooperative RBC to general MISO CBC, the results for single

antenna AWGN partially cooperative RBC in the paper [30] CAN NOT be extended to the MISO AWGN CBC due to the non-degradedness nature of the multi-antenna broadcast channel. Indeed, in the paper [30], the derivation of the results for single antenna AWGN partially cooperative RBC is based on the equivalent degraded representation of Y_2 as the degraded version of a newly defined output, but there is no way for such manipulations to work for the MISO system, which is neither degraded nor equivalent to be degraded.

Remark 3: In the proof, I extend considerations to the complex field.

When CSI is known only at the receiver (CSIR), I allocate power equally over all transmit antennas. If independence is required among all transmitted substreams, I have $\mathbf{Q_X} = \frac{P}{M}\mathbf{I}$ and the region given in (3.2) is reduced to:

Corollary 1. An outer bound on the capacity region of the MISO AWGN CBC with CSIR ($\mathbf{Q_X} = \frac{P}{M}\mathbf{I}$), denoted as $C_{CSIR}^{(o)}$, conditioned on channel realization $\mathbf{h}_1$, $\mathbf{h}_2$ and h_3, is given by

$$C_{CSIR}^{(o)} = \bigcup_{0\le\alpha,\varphi\le 1} \left\{ \begin{array}{ll} R_1 < & \mathcal{C}\left(\frac{\bar{\alpha}\varphi\frac{P}{M}\mathbf{h}_1\mathbf{h}_1^H}{\alpha\frac{P}{M}\mathbf{h}_1\mathbf{h}_1^H+N_0}\right) \\ R_2 < & \min\left\{ \begin{array}{l} \max\limits_{\substack{\mathbf{q_X}x_1: \\ |\mathbf{q_X}x_{1,i}|^2\le\bar{\varphi}\bar{\alpha}P_1\frac{P}{M}}} \mathcal{C}\left(\frac{\tilde{\mathbf{h}}_2\tilde{\mathbf{Q}}\tilde{\mathbf{h}}_2^H}{N_0}\right), \log\left(\det\left(\mathbf{I}+\frac{(1-\bar{\varphi}\bar{\alpha})P}{MN_0}\tilde{\mathbf{H}}\tilde{\mathbf{H}}^H\right)\right) \end{array} \right\} \end{array} \right\}, \tag{3.3}$$

where $\tilde{\mathbf{Q}} = \begin{bmatrix} \frac{P}{M}\mathbf{I} & \mathbf{q}_{\mathbf{X}X_1} \\ \mathbf{q}_{\mathbf{X}X_1}^H & P_1 \end{bmatrix}$.

3.4 Conclusions

An outer bound is derived in this chapter for the capacity region of MISO AWGN cooperative broadcast channels, where the source employs an antenna array to communicate with two single antenna destinations and the stronger destination serves as relay to the weaker destination. With the derived outer bound, we can analyze the lower bound for the outage probability, based on which the diversity-multiplexing tradeoff, defined and studied in the seminal paper [36,37], can be obtained. This has been left to my future work. Also, I am going to consider half-duplex cooperative

communication, which is more practical than full-duplex cooperative communication assumed in this chapter.

CHAPTER 4

IMPLEMENTING INDOOR POSITIONING ALGORITHM VIA ZIGBEE DEVICES

4.1 Introduction

Indoor positioning has many applications in smart offices and homes, and in industrial automation and control. Although it is very common to use GPS for positioning in the open field wherever you are hiking in the mountain or driving on the highway, it is very difficult to apply GPS inside the buildings, because the GPS signals cannot penetrate most roofs covering the buildings. When wireless networks are present, cooperative positioning, which is to estimate the location via the relative distance between two nodes, is emerging as a promising quickly-deployed indoor positioning technology that exploits the ad-hoc network structure. Therefore, the relative distance between nodes plays a crucial role in cooperative positioning. In [38], it claims that there are four physical variables, i.e. the received signal strength indicator (RSSI), the angle of arrival (AOA), the time of arrival (TOA) and the time-distance of arrival (TDOA), to determine the relative distance or range measurements. In most applications of indoor positioning, RSSI obtained by measuring the received wireless signal and TOA obtained by detecting the ultra-sound waves are quite often used to obtain the locations of nodes.

RSSI rather than TOA is studied in this chapter to obtain the relative distance since it does not always be guaranteed that the line-of-sight path exists between nodes in indoor environments. There are three algorithms to computer the coordinates with the help of these relative distance data. One algorithm is called classical Multidimensional Scaling (MDS), a technique that captures the intercorrelation of

high dimensional data at low dimension. MDS has been found in a variety of applications, not limited to computer science or electrical engineering areas [39]. However, for both non-iterative and iterative methods, the classical MDS is sub-optimal because it does not consider the channel statistics and usually measurements of longer distance have larger errors [40]. Another algorithm is called Maximum Likelihood Estimation(MLE) which can achieve the optimum estimation for indoor positioning based on the received signal power, whose distribution is assumed to be known [41]. Due to its computational complexity to obtain closed-form solutions, gradient methods are usually used to iteratively find the global maximum. However, these methods are sensitive to the initial values. We combine MDS and MLE methods by applying MDS to obtain coarse initial values for the MLE iterations. The initial values obtained by MDS are expected with certain confidence to be able to converge to the global maximum.

After introducing the technology of indoor positioning algorithms, we should find a protocol to implement them. As a popular and standard wireless protocol, ZigBee [42,43] is designed as a low-cost, low-power and low-data rate networking technology for Industrial-Scientific-Medical(ISM)-band radio that welcomes even the simplest home and industrial end devices into wireless connectivity. In this work, we set up an indoor positioning system using ZigBee devices. The related work has been done in [44], where the authors claimed to have built a model for monitoring the positions of mobile nodes in an indoor environment according to IEEE 802.15.4 (ZigBee) by using RSSI. But the authors did not point out how to combat the in-building signal fading. A practical ZigBee model for indoor positioning system is provided in [45], which employed both the RSSI and TOA to compensate each other to get the accurate distance for indoor positioning. However, it did not solve how to determine the location if there is no line-of-sight path.

Furthermore, ZigBee technology can determine crucial parameters, such as path loss exponent (e.g.,n,γ,etc.) in a classical statistical log-normal indoor channel model [46] which is adopted in our simulations. In order to provide convincing simulation

results, our channel model used in the simulation is based on real measurements obtained by our lab's ZigBee system evaluation devices, and we also developed our own ZigBee codes for real-time indoor channel RSSI measurements.

The whole project goes like this: The first step is to find an effective and efficient algorithm via simulations. Then, some crucial parameters in channel model to support simulations are obtained from the real measurements reported by ZigBee devices. Finally, a hardware ZigBee testbed is built to evaluate the indoor positioning algorithms, softwares and hardwares. To respond to this procedure, the remaining of this chapter is organized as follows. In the section 4.2, three positioning algorithms including the proposed algorithm in this chapter are described and compared . How to evaluate the goodness of an algorithm is presented in the section 4.3. After a classical statistical log-normal indoor channel model is introduced, some real measurements from ZigBee devices for indoor channel model is shown in the section 4.4. In the section 4.6, a testbed is described in detail. Simulation results are provided in the section 4.5. Last but not least, future work and conclusion are addressed in the section 4.7.

4.2 Positioning Algorithms

The cooperative positioning problem is to estimate the coordinates $x_{i_{i=1}}^{N}$ i=1 of the N network nodes, given imperfect knowledge of pair-wise range measurements and the coordinates of the reference nodes.

4.2.1 Classical-MDS

This algorithm is derived from the classical multidimensional scaling algorithm in [40]. First of all, we need the true Euclidean distances between N nodes:

$$d_{ij} = d(x_i, x_j) = \sqrt{(x_i - x_j)^T (x_i - x_j)}, i, j = 1 \ldots N \tag{4.1}$$

The squared distance matrix can be defined as $D = [d_{ij}^2]$. In order to get the solution from this matrix by singular value decomposition (SVD), we need to define H as $H = I - ee^T/N$, where e is an N-dimensional all-ones vector. Next, a matrix B' is introduced for solving the equation:

$$B' = -HDH = 2HX^TXH = (\sqrt{2}XH)^T(\sqrt{2}XH).$$

Then, the floating coordinates can be obtained as solutions to the following problem:

$$\min_Y ||B' - Y^TY||_F^2 \tag{4.2}$$

where $||.||_F$ is the Frobenius norm. The solution of (4.2) is given by

$$X = diag(\lambda_1^{1/2}, \ldots, \lambda_D^{1/2})U^T/\sqrt{2} \tag{4.3}$$

where $\lambda_1^{1/2}, \ldots, \lambda_D^{1/2}$ and U are from SVD decomposition of B' as:

$$B' = Udiag(\lambda_1^{1/2}, \ldots, \lambda_D^{1/2})U^T$$

Although this classical MDS would involve much computation mainly due to SVD operation in a large dimension network where there many nodes for position estimation, its performance is not bad for small scale estimation. As a rule of thumb, small scale refers to the number of nodes to be estimated being less than 6. It enlightens us that the classical MDS is a good initial estimation because it is a linear estimation and it does not need the initial value on its own. Figure 4.1 shows the positioning results using the classical MDS. In this figure, the red dots are the real nodes locations, black diamonds are the mean value of the estimated nodes locations, red dash circles are the Cramér-Rao bound and black ellipses are the variance of the estimated nodes locations. The blue squares denote the locations of known nodes. The number marked on the figure is the average of all estimation variances. Cramér-Rao bound is the most famous lower bound for unbiased variance [47]. It can be used a benchmark to help us evaluate the potential of an estimator.

As well known, CR bound is by far prevailing boundary for MVUE compared with other variance bounds [48]. In [49], there is a perfect derivation of CR bound

for indoor positioning. Here, a very brief derivation is provided according to [48,49]. A Fisher Matrix can be obtained by:

$$\mathbf{I}(\boldsymbol{\theta}) = \begin{bmatrix} \mathbf{I_{xx}} & \mathbf{I_{xy}} \\ \mathbf{I_{xy}^T} & \mathbf{I_{yy}} \end{bmatrix} \tag{4.4}$$

We can find the variance of x and y by: $var(\hat{\theta}_i) \geq [\mathbf{I^{-1}}(\theta)]_{ii}$ and apply the equation for inverse of matrix as follow:

$$\begin{bmatrix} A & U \\ V & D \end{bmatrix}^{-1} = \begin{bmatrix} (A - UD^{-1}V)^{-1} & -(V - DU^{-1}A)^{-1} \\ (U - AV^{-1}D)^{-1} & (D - VA^{-1}U)^{-1} \end{bmatrix} \tag{4.5}$$

[50] Therefore, from (4.4)(4.5), we can get:

$$\begin{aligned} var(\hat{\theta}_i) &\geq [\mathbf{I^{-1}}(\theta)]_{ii} \\ &= [(\mathbf{I_{xx}} - \mathbf{I_{xy}}\mathbf{I_{yy}}^{-1}\mathbf{I_{xy}}^T)^{-1}]_{ii} \\ &\quad +[(\mathbf{I_{yy}} - \mathbf{I_{xy}}^T\mathbf{I_{xx}}^{-1}\mathbf{I_{xy}})^{-1}]_{ii} \end{aligned} \tag{4.6}$$

CR-bound provide a frontier of most estimation for indoor positioning as well as some interesting conclusions, among which one of the most important is that even more unknown nodes can still improve the accuracy of indoor estimation by cooperative way.

The classical MDS solution is *floating* and can not point out the location of nodes directly. We propose an approach which contains three steps to convert the *floating* solution to *fix* solution. Details are described in the section 4.3.

4.2.2 Iterative-MDS

Besides the classical MDS, we can use the iterative approach to solve the MDS problem as well as Eq. (4.2). Firstly, a cost function defined in [39] is as follows:

$$S = \sum_{1 \leq i \leq n} \sum_{1 < j \leq n} (r_{ij}^{(t)} - d_{ij})^2, \tag{4.7}$$

where d_{ij} is the actual Euclidean distance as defined in (4.1) and the $r_{ij}^{(t)}$ is measured distance at t-th iteration.

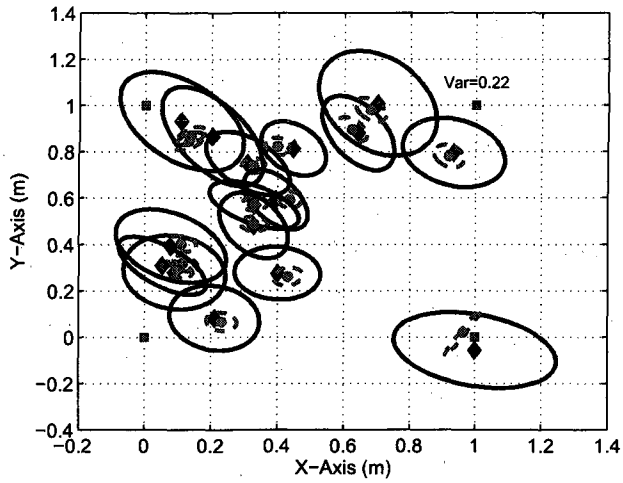

Figure 4.1. Estimated by classical-MDS.

S can be rewritten as

$$S = \sum_{i=1}^{n} S_i + c \tag{4.8}$$

where S_i is the local cost function and c is a constant which has nothing to do with cost function. According to [51], S_i can be expressed as

$$S_i(x_i) = \eta_r^2 + \eta^2(X) - 2\rho(X). \tag{4.9}$$

Define $T_i(x, y)$ as:

$$T_i(x_i, y_i) = \eta_r^2 + \eta^2(X) - 2\rho(X, Y) \tag{4.10}$$

where $\rho(X, Y)$ is

$$\rho(X, Y) = \sum_{\substack{j=1 \\ j \neq i}}^{n} \frac{\overline{r}_{ij}}{d_{ij}} (x_i - x_j)^T (y_i - y_j) \tag{4.11}$$

According to Cuachy-Schwarz inequality, it is obtained that

$$d_{ij}(X) = \frac{d_{ij}(X) d_{ij}(Y)}{d_{ij}(Y)} \geq \frac{(x_i - x_j)^T (y_i - y_j)}{d_{ij}(X)} \tag{4.12}$$

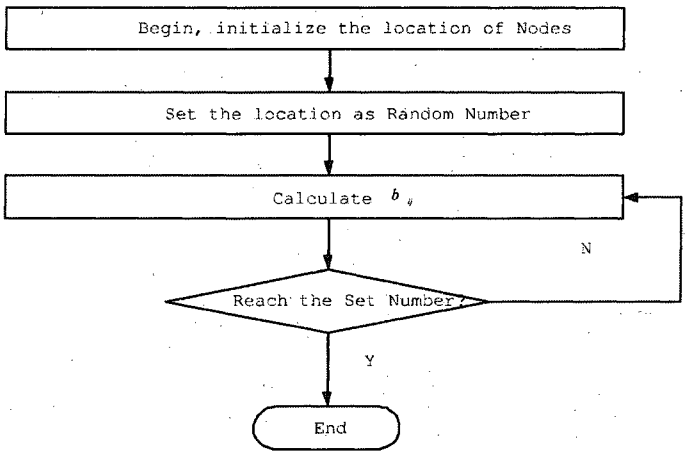

Figure 4.2. Procedure of iterative-MDS algorithm.

Obviously, in order to find $T_i(x, y)$, the S_i needs to be minimized by a majorizing algorithm:

$$\frac{\partial T_i(x_i, y_i)}{\partial x_i} = 0 \tag{4.13}$$

We can derive a location of node i through (4.13)

$$x_i^{(k+1)} = a(d_i \bar{x}_i + X^k b_i^k), \tag{4.14}$$

where, a is $N-1$ and b_i is obtained iteratively.

The detailed procedure is shown in Figure 4.2.

4.2.3 Maximum Likelihood Estimation

In this section, we reintroduce the main point of the paper [41] about the Maximum Likelihood formulation for indoor positioning without considering the threshold. Here, we have a likelihood function L.

$$L = \prod_{i=1}^{N} \prod_{j \neq i} \left\{ \exp \left[-\frac{1}{2} \left(\frac{p_{i,j} - \hat{p}_{i,j}}{\sigma_{dB}} \right)^2 \right] \right\}, \tag{4.15}$$

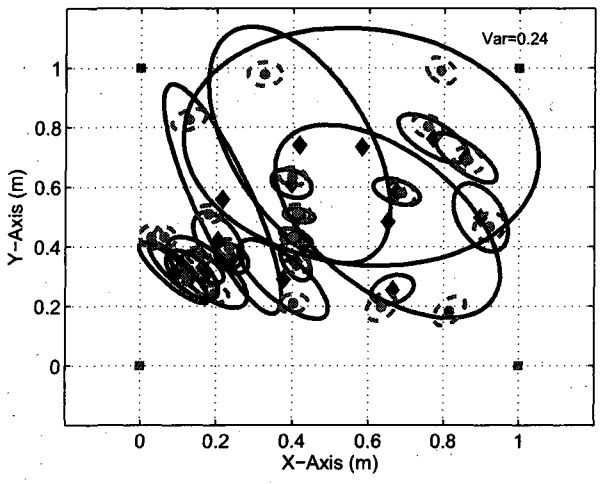

Figure 4.3. Estimated by MLE.

where $\hat{p}_{i,j}$ represents the power received by device i that was transmitted from device j and $p_{i,j}$ is the postulated received power. The ML coordinates are given by

$$X, Y = \arg\min_{X,Y} \left[f\left(x_k, y_k\right) \right] \tag{4.16}$$

$$f\left(x_k, y_k\right) = \frac{a^2}{8} \sum_{i=1}^{N} \sum_{j \neq i} \ln^2 \frac{\hat{d}^2}{d_{i,j}^2} \tag{4.17}$$

where,

$$a = 10n/(\ln(10)\sigma_{dB})$$

We can use the iterative methods, say conjugate gradient or Newton-Raphson iteration [48], to solve (4.17). MLE is a very powerful estimator which provides near CR-bound estimation for indoor positioning using the proper initial estimation. However, like everything has two sides, MLE has its own drawback. For instance, it is sensitive to initial estimated values. Figure 4.3 shows the localization results using the MLE with random initial guess. You may see that MDS alone or MLE with random initial value alone works not very well. We should figure out a new and better algorithm for indoor positioning.

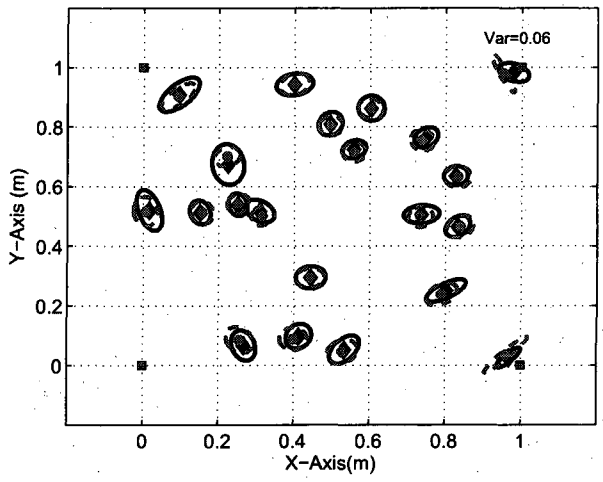

Figure 4.4. Estimated by combination algorithm.

4.2.4 Combination Algorithm

We combine the above algorithms for better performance, i.e. the MDS is used to obtain the initial values for the MLE. In the implementation, we divide the unknown nodes into groups. With the reference nodes, each group is applied the classical MDS, which does not need any initial values. This approach can ease the computation of performing SVD on large B'. The coordinates estimated using MDS are fed to the MLE as the initial guess.

4.3 Evaluations

Almost every paper on indoor positioning needs to find a standard to evaluate their algorithm in order to claim their results. Most of them prefer to select or design some fix points to be reference points [52–54]. However, which points are selected or how those points are selected can affect the final conclusions very much. Actually, in a real indoor radio propagation environment, it is very difficult to define a standard statistics fix point distribution to be accepted by other researchers. So the theories

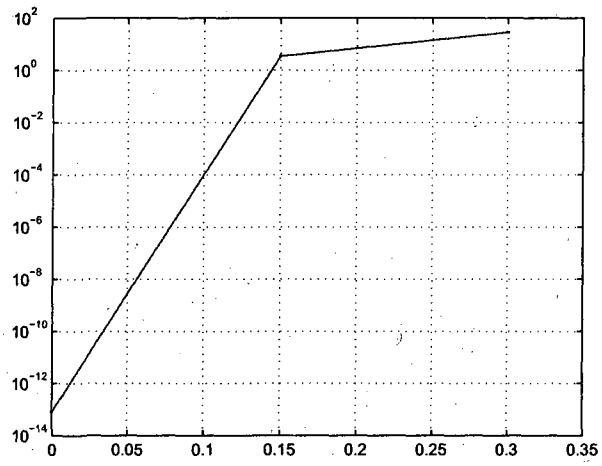

Figure 4.5. Position error.

or algorithms are not very convincing if they are based on the particular fix point model. In some cases, we just care the structure of the nodes. It is a task for us to find an easy, fast, and objective approach to evaluate indoor positioning algorithms.

We proposed a quick way to carry out the evaluation by obtaining the Root Mean Square Error (RMSE) of estimated distance. The procedure of that RMSE evaluation is that we calculate the *floating* solution by SVD again to get the distance distribution matrix. Compared with direct position error, RMSE of distance provides a quick evaluation without losing the key information although it is not a direct way. Figure 4.6 shows the RMSE of distance and Figure 4.5 shows the direct position error. We observe that they look very similar in shape though the values at y-axis are different. However, some people do not like this indirect evaluation because they want to get some accurate benchmark.

The challenge of comparing the *floating* solution lies in the issue of topology. In most of existing works, the authors use some fix or known points as their evaluation's anchor or reference points. In this proposal, we proposed another innovative evaluation method without using the fix or known points so that we can improve efficiency.

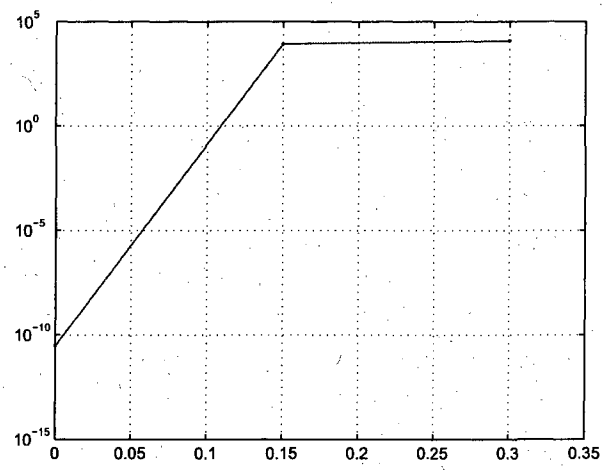

Figure 4.6. RMSE distance error.

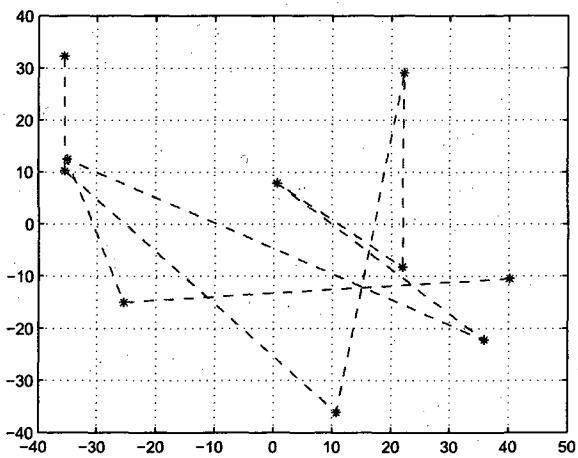

Figure 4.7. Original nodes location.

This evaluation includes three steps. Firstly, we obtain the *floating* solution by SVD or by iteration and find the mass centric point of original location and calculated location by calculating the mean value of x and y coordinator. After we adjust their mass centric point to original point, we get the Figure 4.7 and Figure 4.8.

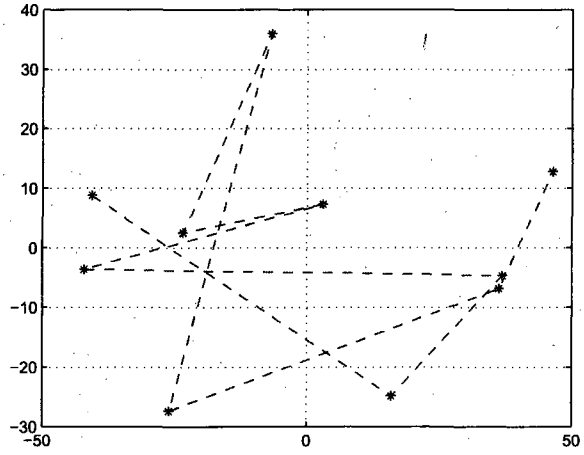

Figure 4.8. Floating solution by classical-MDS.

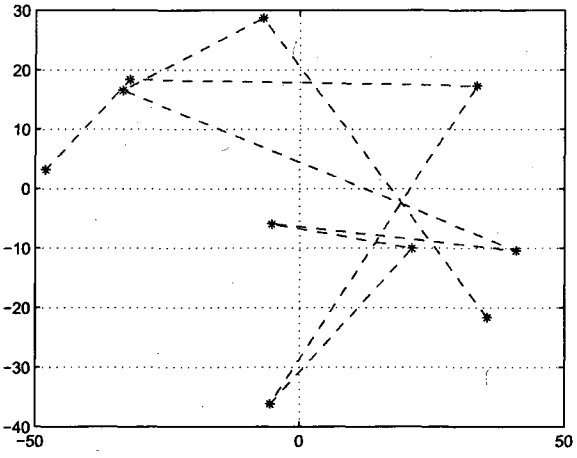

Figure 4.9. After rotating.

In the second step, we connect each point with the original point and find their angle and calculate the average angle. By comparing the two average angles, we get the angle difference to be a rotation angle. See Figure 4.9.

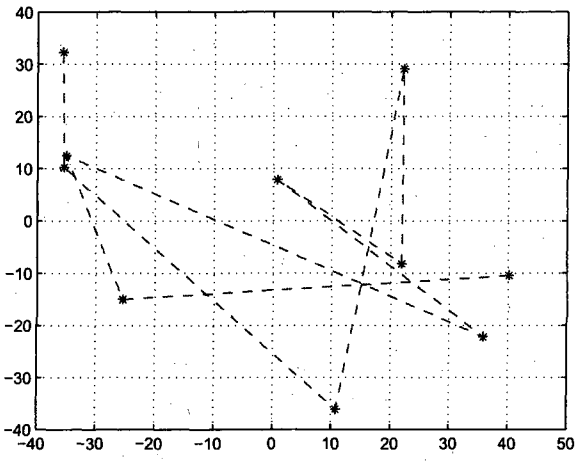

Figure 4.10. After rotating and flipping.

Finally, in the third step, we check whether it needs the mirror flipping. In some cases, we do not need to flip the *floating* solution but in other cases, we must flip them. See Figure 4.10.

Comparing the Figure 4.10 and Figure 4.7, we find that they look almost the same, which indicates the the floating solution is extremely accurate and this is because the *floating* solution is obtained without any noise and interference. We also know that this innovative evaluation can provide us a quick answer for the similarity between the original location and solved location.

4.4 Channel Model

This section is focusing on the implementation of indoor positioning by ZigBee devices. There are a lot of statistical channel models, such as Okumura Model [55] and Hata Model [56], etc. Here are two famous channel. The one is the TOA channel:Let $T_{i,j}$ be the measured TOA between nodes i and j in seconds. Assume that $T_{i,j}$ is Gaussian distributed, i.e.

$$T_{i,j} \sim \mathcal{N}(d_{i,j}/c, \sigma_T^2), \tag{4.18}$$

where c is the speed of light and σ_T^2 is a constant which does not vary with $d_{i,j}$, the distance between nodes i and j. Then, the MLE based on TOA is given by

$$\hat{\theta} = \arg\min \sum_{i=1}^{N-1} \sum_{j=i+1}^{N} (cT_{i,j} - d_{i,j})^2 \tag{4.19}$$

The other is LOG-NORMAL channel: We adopt a log-normal distribution channel model [57], by assuming that there are plenty of objects between two nodes and considering central limit argument. Among all cases, the log-nomal channel is the hardest. So, the log-normal is focused in this thesis. A very classical statistical channel model in [46] was presented as follows :

$$P_{ij}(dBm) \sim N(\bar{P}_{ij}(dBm), \sigma_{dB}^2)$$

$$\bar{P}_{ij}(dBm) = P_0(dBm) - 10n_p log_{10}(d_{ij}/d_0) \tag{4.20}$$

where $\bar{P}_{ij}$ is the mean value of received decibel power corresponding to a specific distance d_{ij} and σ^2 is the variance of degradation. P_0 and d_0 are the reference power and distance respectively. n_p, called pass loss exponent, is a crucial parameter which will be discussed in detail later. It is not very hard to get the estimation $\hat{d}_{ij}$ of real distance d_{ij} by the maximum likelihood estimator:

$$\hat{d}_{ij} = d_0 10^{(P_0 - P_{ij})/(10n_p)} \tag{4.21}$$

Define $X_\sigma = \bar{P}_{ij} - P_{ij}$, then $X_\sigma \sim N(0, \sigma^2)$. Rewrite the (4.21), and we can get:

$$X_\sigma[dB] = 10nlog(\frac{\hat{d}_{ij}}{d_0}) - 10nlog(\frac{d_{ij}}{d_0}) \tag{4.22}$$

$$\hat{d}_{ij} = d_{ij} 10^{X_\sigma/(10n_p)} \tag{4.23}$$

Equation (4.23) is a basic mathematic description for model used in this work. Although the range of n_p can be found in many textbooks [58], we need a specific value of n_p to support convincing simulations.

ZigBee devices provide a good platform to obtain the indoor wireless channel measurements and thus we use the ZigBee devices as fundamental hardware devices

for indoor positioning to estimate distance between the transmitter and the receiver based on the received signal power, since the received signal strength indicator (RSSI) can be linearly related to a ZigBee parameter, the link quality indicator (LQI). For example, using the Jennic JN5139 module,

$$i16RSSI = ((u8LQI * (880000000/255))/10000000) - 98 \tag{4.24}$$

where, $i16$ and $u8$ denote 16-bit integer and 8-bit unsigned integer, respectively, in the C programming language. According to (4.24), power levels below about -101 dBm and above -14 dBm are not differentiated. The accurate range is checked from -98 dBm to -10 dBm. In reality, the LQI is a coarse and quantized indicator, and the localization accuracy is greatly deteriorated by the harsh indoor channel conditions due to walls, irregular room shapes, and other obstacles. Sophisticated ZigBee codes are required for LQI with unreliable range measurements, yet its complexity is restricted in order to fit the simple ZigBee profile. For indoor wireless channel measurement, we have tested a $20m \times 20m$ hall many times. The results are listed as a table in Figure 4.11, where LQI_A to LQI_D are LQI values measured at the same specified distance. The variation in the values are due to the indoor shadowing. The probabilities of LQI_A to LQI_D are 0.35,0.35,0.2 and 0.1. So the average LQI (in the same row) is calculated as:

$$LQI = 0.35 * LQI_A + 0.35 * LQI_B + 0.2 * LQI_C + 0.1 * LQI_D \tag{4.25}$$

According to (4.23),(4.24) and (4.25), n_p=3.5767 is obtained by selecting distance 1m and 2m to calculate the n_p as follows:

$$p1 = ((159.3 * (880000000/255))/10000000) - 98$$

$$p2 = ((128.1 * (880000000/255))/10000000) - 98$$

$$n_p = (p1 - p2)./10./log_{10}(2/1)$$

As shown in Figure 4.12, the red curve based on (4.23), (4.24) and (4.25) is a good match with the black curve of actually measured indoor LQI.

LQI	Distance	LQI_A	LQI_B	LQI_C	LQI_D
165.9	0.5	168	162	174	156
159.3	1	162	156	162	156
141.6	1.5	144	144	138	132
128.1	2	126	132	120	138
111.9	3	108	114	120	102
105.9	3.5	102	108	114	96
90.6	4	90	90	96	84
83.4	5	84	84	78	90
73.5	6	72	78	72	66
72.6	7	72	72	78	66
65.7	8	66	72	60	54
65.4	9	66	72	60	72
61.5	10	66	66	60	54
56.1	11	60	60	48	66
51.3	12	54	54	54	48
47.4	13	48	48	42	54
44.7	14	42	48	42	48
38.7	15	36	42	36	42

Figure 4.11. LQI measurements.

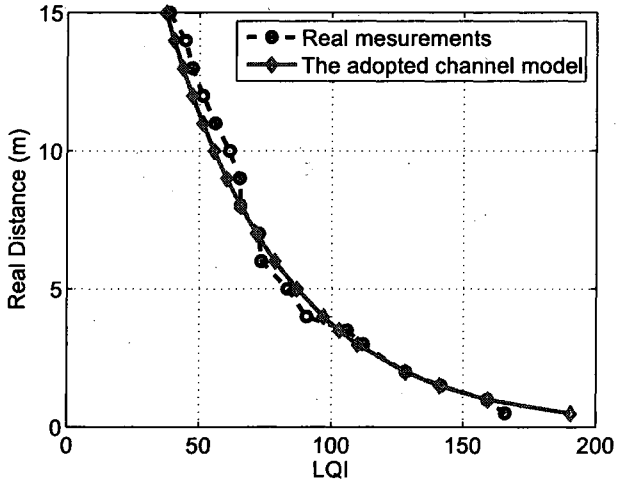

Figure 4.12. Distance vs LQI.

4.5 Numerical Results and Analysis

Now, we have built a convincing channel model based on real measurements. With that channel model and an innovative evaluation approach proposed by us, we can conduct some research to get some significant conclusions to direct our future work.

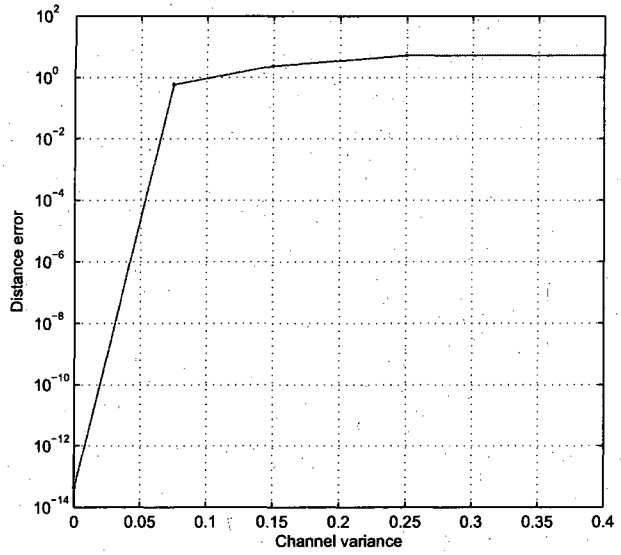

Figure 4.13. Distance error versus channel variance.

In Simulation One (Figure 4.13), the x-axis is channel variance and y-axis is the distance error. We may see that it is very steep in the first part and quite flat in the second part. This means the distance error is very sensitive to channel variance. Whatever channel measurement you use, such as UWB [59], Ultra-sonic [60] and radio signal, if you can not guarantee the accuracy of the measurement, you can not obtain the accurate position whatever advanced algorithms you employ.

The definition of x-axis and y-axis for Figure 4.14 are the same as in Simulation One Figure 4.13. The red curve is the performance of Iterative-MDS algorithm, and blue curve is the performance of the classical-MDS algorithm. We may see that the classical-MDS algorithm is a little better than the iterative-MDS in the steep part and they are very close in the flat part. Therefore, although the classical-MDS performs better than the iterative-MDS, considering the algorithm complexity, we choose Iterative-MDS in practice to avoid large dimension matrix decomposition

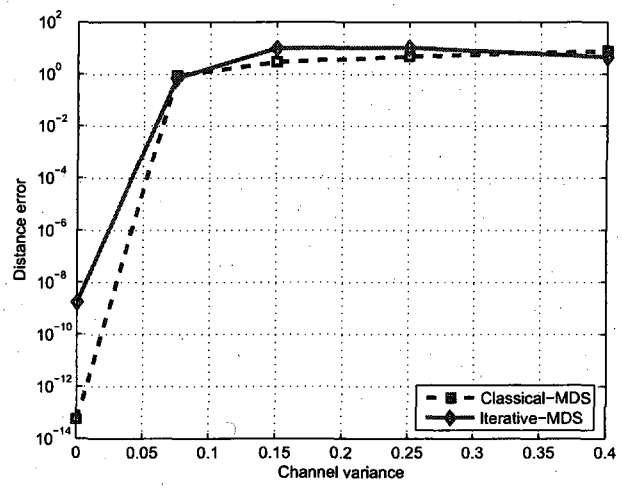

Figure 4.14. Comparison of classical-MDS and iterative-MDS.

needed in the classical-MDS. Besides, the iterative-MDS can be applied in many real-time systems.

The estimation performance of all algorithms is compared in Figure 4.15. It shows that as the number of unknown nodes increases, on average, the MDS outperforms the MLE with random initial values. The proposed combination algorithm, i.e. MDSMLE, works well for the indoor environments, as its estimation performance is close to the CR bound.

4.6 Testbed

We developed a ZigBee testbed for indoor positioning experiment. See Figure 4.16. The program running in laptop computer is coded by Visual C++ to verify positioning algorithms. The red square marks the running window and details are shown in Figure 4.17. The window that displays the LQI data sent from ZigBee coordinator is highlighted by a black oval. Green square denotes the ZigBee coordinator and ZibBee end nodes are marked by blue circles. All LQI data from ZigBee coordinator go through the serial cable and reach the laptop computer. See the yellow circle. Laptop

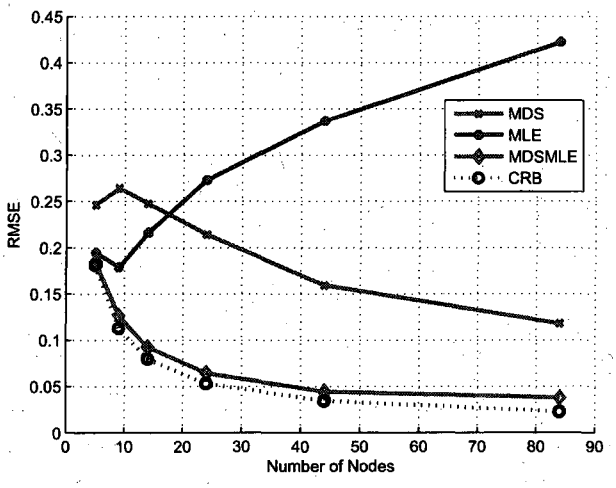

Figure 4.15. Comparison of positioning algorithms.

computer plays a role as a central processor and monitor. The ZigBee testbed is running in the lab as shown in Figure 4.18. The testbed consists of an ad-hoc network of the ZigBee coordinator and end nodes marked by the red circles. The coordinator is connected with a laptop computer which can display the calculated relative positions in real-time (Figure 4.17). In its first phase, the cooperative algorithm is centralized and installed in the laptop. The ZigBee coordinator collects the LQIs among network nodes and sends them to the laptop. In later phases, the cooperative algorithm will be implemented in the coordinator equipped with ZigBee design-in modules and be distributed to mesh nodes with ZigBee chipset reference designs.

In addition to evaluating the algorithms mentioned in this chapter, this testbed can provide an ideal platform to verify and compare other indoor positioning algorithms. Moreover, it has paved the road to create a real industrial product for indoor positioning via ZigBee devices.

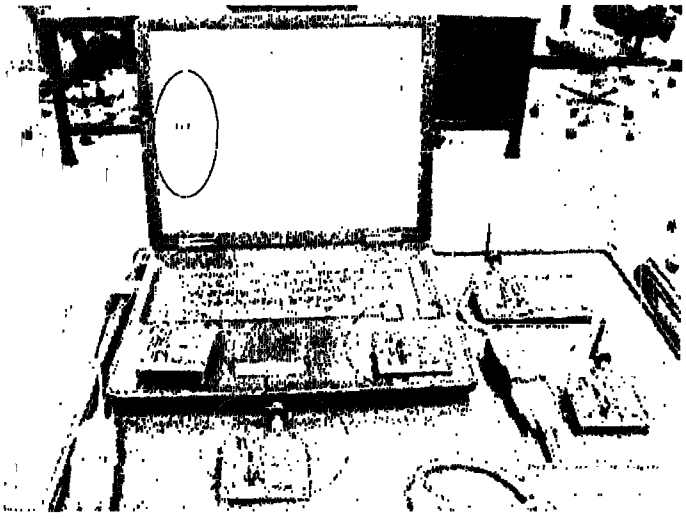

Figure 4.16. Structure of testbed.

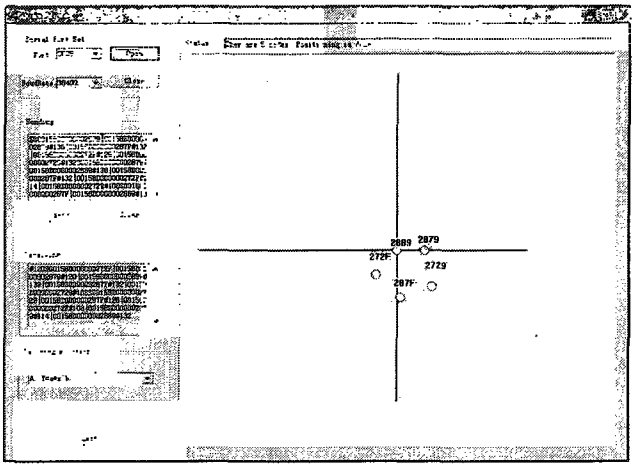

Figure 4.17. Screen of testbed.

4.7 Conclusions and Future Work

We developed an indoor positioning system that uses wireless ZigBee devices. It implements the cooperative localization algorithm and uses the RSSI as node pairwise range measurement.

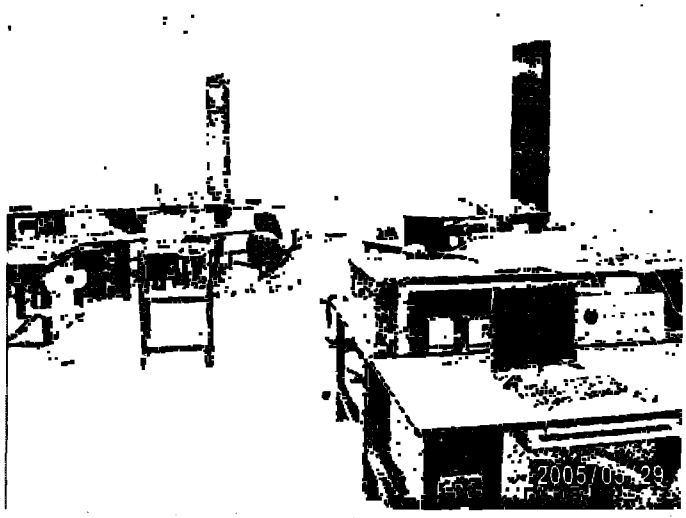

Figure 4.18. Testbed is running.

Using the testbed, the LQIs of the network were measured in several indoor environments. The measurement data were used to examine the lognormal channel model, and calculate model parameters for each particular indoor environment. We proposed a cooperative localization algorithm that combines MDS with MLE for optimal performance. In our future work, we will develop the real-time aspect of the system to estimate node positions based on measurement data, and more accurate positioning algorithm to the network.

CHAPTER 5

MMSE COOPERATIVE POSITIONING ALGORITHM IN WIRELESS NETWORKS

5.1 Introduction

Positioning via GPS is also quite challenging in some hostile environments where the GPS signals could be jammed. So, quite extensive work has been done to study non-GPS positioning methods to locate a node in a wireless network. There are two classes of non-GPS positioning methods: non-cooperative methods or cooperative methods. In non-cooperative methods, the position of an individual node is estimated without taking into consideration the information related to other nodes. A traditional non-cooperative method that can be traced back to ancient times is to locate an unknown node using its distance with three anchor nodes. The obtained estimated positions can be polished using fuzzy mathematics as proposed in [61]. In cooperative methods, the position of any node is estimated based on the complete information concerning all nodes. Obviously, the cooperative position estimator makes the best use of all available information and thus is superior to the non-cooperative estimator. So, we focus our study on cooperative positioning approaches.

Estimating positions based on Multi-Dimension-Scaling (MDS) techniques [39] is a well known cooperative positioning method. MDS captures the intercorrelation of high dimensional data at low dimension. It has many applications not only in the areas of computer science and electrical engineering but also in a variety of other areas, such as chemical modeling, political science, etc. In MDS positioning method, the coordinates of all unknown positions are solved as the least square solutions to an overdetermined equation set formed using all distances between each pair of

nodes. The singular value decomposition (SVD) is commonly used to obtain the MDS solutions. Details of solving MDS via SVD can be found in our previous work [62].

Another very popular cooperative positioning method is the Maximum Likelihood Estimation (MLE) estimator which has been studied extensively in [41,49,63,64]. An online program can be found in [65] as a supplement to these works. It has been shown in these works that MLE is an asymptotic unbiased estimation that is asymptotically efficient since its variance is close to the Cramér-Rao bound (CRB). Due to the complicated likelihood expression, no analytical formulas can be established for the maximizer of the likelihood function, so the MLE position estimator has to be solved iteratively via numerical methods, such as the conjugate gradient or the Newton-Raphson technique [66]. However, since this is not a convex optimization problem, it is not guaranteed that global maximizer can be achieved starting with any initial estimation [67]. Details are described in our previous work [62].

One thing common to MDS and MLE is that they are classical estimators and do not take into consideration the a priori distribution of the true positions. Better estimators can be obtained via Bayesian estimation by treating the true positions as random unknown parameters distributed according to a priori Probability Density Function (PDF). This motivates our search for Bayesian cooperative positioning algorithms. In this work, we proposed a cooperative position estimator that minimizes the Bayesian mean squared error (MSE). The proposed estimator is thus called *MMSE cooperative position estimator.*

The positioning algorithm based on the Extended Kalman Filter (EKF) [48] also belong to Bayesian estimators. Some variations of the extended Kalman method can be found in [68]. While the EKF estimators are applied to track the position of a single moving node using the updated state information, our MMSE estimator is used to locate multiple nodes in a cooperative way.

Detailed derivation for the proposed MMSE estimator is provided in this work. Its performance is thoroughly studied in terms of the bias, variance and MSE, and is compared with the performance of MLE and MDS, two most popular existing position

estimators introduced previously. The CRB is also computed and used to evaluate the MMSE estimator's performance. We also proposed several variations of the basic MMSE estimator to improve performance. For wireless networks of a large number of nodes, the proposed MMSE cooperative estimator can be integrated with other estimators, such as MLE, to achieve excellent performance at low computation cost.

This chapter is organized as follows. The system model, especially the channel model, is described in the section 5.2. A very classical channel model is adopted and its important parameters are obtained based on real measurements. In the section 5.4, the proposed MMSE cooperative positioning algorithm is derived and studied. Based on study in the section 5.4, several variations of the original MMSE estimator are proposed in the section 5.5. The superior performance of the proposed MMSE estimator and its variations is further verified by the simulation results presented in the section 5.6. Future work and conclusion of this chapter are addressed in the section 5.7.

5.2 System Model

Consider a wireless network of N unknown nodes and M anchor nodes. The position for any unknown node i, $1 \leq i \leq N$, is described by its coordinates (x_i, y_i). The power degradation between any pair of nodes is observed to estimate the coordinates of unknown nodes.

Let P_{ij} denote the power loss between the node i and the node j, whose distance is denoted as d_{ij}. P_{ij} usually varies for the same value of d_{ij}, therefore it is treated as random. As in [57], we adopt the classical log-normal distribution [46], which is based on the assumption that there are plenty of objects between two nodes and is thus justified by the central limit theorem. Thus, we have

$$P_{ij}(dB) \sim \mathcal{N}\left(\bar{P}_{ij}(dB), \sigma_{dB}^2\right) \tag{5.1}$$

where $\bar{P}_{ij}(dB)$ is the expectation corresponding to the specific d_{ij} and the variance σ_{dB}^2 keeps the same for any distance. Suppose the average power degradation at distance

d_0 is $P_0(dB)$. P_0 and d_0 are called the reference power and distance respectively. According to [46], we have

$$\bar{P}_{ij}(dB) = P_0(dB) - 10n_p log_{10}\left(\frac{d_{ij}}{d_0}\right), \tag{5.2}$$

where n_p is the *path loss exponent.*

After suffering laborious field tests, n_p=3.5767 is acquired eventually. Details can be found in our previous work [62]. It is also noted that the model (5.2) matches the field measurements very well.

5.3 MAP Cooperative Positioning

Depending on different cost functions, the Bayesian estimators consist of two major estimators, one of which is MAP, the other is MMSE, discussed by following next section.

It is not very hard to prove that famous MLE is equivalent to MAP. The proof is given as follows:

Proof

$$\begin{aligned}
MAP &= \max(PosteriorPDF) \\
&= \max[f(\boldsymbol{\theta}|\mathbf{P})] \\
&= \max\left[\frac{\prod_{i=1}^{N}\prod_{j<i}\exp\left(\frac{a}{8}ln^2\frac{d_{ij}^2}{\hat{d}_{ij}^2}\right)}{\int\cdots\int\prod_{i=1}^{N}\prod_{j<i}\exp\left(\frac{a}{8}ln^2\frac{d_{ij}^2}{\hat{d}_{ij}^2}\right)d\boldsymbol{\theta}}\right] \\
&= C_{map}\max\left[\prod_{i=1}^{N}\prod_{j<i}\exp\left(\frac{a}{8}ln^2\frac{d_{ij}^2}{\hat{d}_{ij}^2}\right)\right] \\
&= \max\left[\prod_{i=1}^{N}\prod_{j<i}\exp\left(\frac{a}{8}ln^2\frac{d_{ij}^2}{\hat{d}_{ij}^2}\right)\right] \\
&= \max(LikelihoodPDF) \\
&= MLE
\end{aligned} \tag{5.3}$$

where, C_{map} is a constant value and equals to $\left[\int\cdots\int\prod_{i=1}^{N}\prod_{j<i}\exp\left(\frac{a}{8}ln^2\frac{d_{ij}^2}{\hat{d}_{ij}^2}\right)d\boldsymbol{\theta}\right]^{-1}$

■

Since the MLE is intensively studied by others now, we may jump over the MAP in this thesis.

5.4 MMSE Cooperative Positioning

5.4.1 Basics

In general, for Bayesian estimators, the mean square error (MSE) between unknown random parameter X and its estimation $\hat{X}$ is defined as

$$\text{MSE} \equiv \mathsf{E}[(X - \hat{X})^2], \tag{5.4}$$

where the expectation is taken with respect to both X and $\hat{X}$. MSE defined above is also referred to as *Bayesian MSE* in [48] to distinguish from the MSE of classical estimators, denoted as MSE(X) and defined as

$$\text{MSE}(X) \equiv \mathsf{E}[(\hat{X} - X)^2 | X], \tag{5.5}$$

where the expectation is taken with respect to $\hat{X}$. It is easy to see that MSE = $\mathsf{E}[\text{MSE}(X)]$.

It is well established that, given the a priori distribution for X, the conditional mean of X conditioned on the given observation sample Y minimizes the MSE among all estimators, including linear and nonlinear estimators [48]. That is, the minimum MSE (MMSE) estimator for X, denoted as $\hat{X}_{\text{MMSE}}$, is

$$\hat{X}_{\text{MMSE}} = \mathsf{E}[X|Y]. \tag{5.6}$$

Obviously, the MMSE estimator is a Bayesian estimator.

5.4.2 MMSE Cooperative Position Estimator

Let $\boldsymbol{\theta}_i = (x_i, y_i)$ and its estimate is $\hat{\boldsymbol{\theta}}_i = (\hat{x}_i, \hat{y}_i)$. Then the MSE for the unknown vector parameter $\boldsymbol{\theta} = (\boldsymbol{\theta}_1, \cdots, \boldsymbol{\theta}_N)$ is defined as

$$\text{MSE} = \frac{1}{N} \sum_{i=1}^{N} \mathsf{E}[(x - \hat{x}_i)^2 + (y - \hat{y}_i)^2]. \tag{5.7}$$

We need to find $(\hat{x}_1, \hat{y}_1, \cdots, \hat{x}_N, \hat{y}_N)$ to minimize the total MSE. Since $\hat{x}_i$ is independent from $\hat{y}_i$ for any i and estimators for different node i are independent from each other, it is obvious that minimizing the total MSE is equivalent to minimize $\mathsf{E}[(x - \hat{x}_i)^2]$ and $\mathsf{E}[(y - \hat{y}_i)^2]$ respectively for any i. The observation is all power degradation measurements. According to the previous part, it is straightforward to conclude that by particularizing the general formula (5.6) to our positioning problem, we can obtain the MMSE coordinates estimator $(\hat{x}_{i,\text{MMSE}}, \hat{y}_{i,\text{MMSE}})$ expressed as

$$\begin{matrix} \hat{x}_{i,\text{MMSE}} = \mathsf{E}[x_i|\mathbf{P}] \\ \hat{y}_{i,\text{MMSE}} = \mathsf{E}[y_i|\mathbf{P}] \end{matrix}, \quad i = 1, \cdots, N \tag{5.8}$$

where $\mathbf{P}$ represents the collection of power degradations between each pair of N unknown nodes and between each unknown node and the M anchor nodes, which can be mathematically expressed as

$$\mathbf{P} = (P_{ij} | 1 \leq i \leq N, i+1 \leq j \leq N+M), \tag{5.9}$$

with the node j with $j = N+1, \cdots, M$ referring to one of the anchor nodes.

The MMSE position estimation in (5.8) is a *cooperative* method, since the estimated position for any individual unknown node is obtained based on information concerning other unknown nodes. In contrast, a non-cooperative version of (5.8) would be only conditioned on power degradations between the current node and the anchor nodes, i.e. P_{ij} with $j = N+1, \cdots, N+M$ and thus would have nothing to do with any other unknown nodes.

As in [69] and [70], it is assumed that a node appears randomly with equal probability at any position within a given area and the possible position of any node is independent from that of other nodes. This means that the a priori distribution for $\boldsymbol{\theta}$ is assumed to be independent uniform distribution. Suppose the node i may appear within a rectangular box centered at (O_{ix}, O_{iy}) of $2A_i$ long along x-axis and $2B_i$ long

along y-axis. Then, for $x_i \in (O_{ix} - A_i, O_{ix} + A_i), y_i \in (O_{iy} - B_i, O_{iy} + B_i)$, $1 \le i \le N$, the a priori PDF $f(\boldsymbol{\theta})$ is expressed as

$$\begin{aligned} f(\boldsymbol{\theta}) &= f(x_1, y_1, \cdots, x_N, y_N) \\ &= f(x_1)f(y_1)\cdots f(x_N)f(y_N) \\ &= \prod_{i=1}^{N} \frac{1}{2A_i} \prod_{i=1}^{N} \frac{1}{2B_i}. \end{aligned} \tag{5.10}$$

As derived in Appendix B.1, with the independent uniform a priori distribution (5.10) and the log-normal distribution for power degradation (5.1), the MMSE cooperative position estimator for node i, $1 \le i \le N$, is given as

$$\begin{aligned} \hat{x}_{i,\mathrm{MMSE}} &= \frac{\int_{S_N}\cdots\int_{S_1} x_i \prod_{i=1}^{N}\prod_{j=i+1}^{N+M} \exp\left(-\frac{\alpha}{8}\ln^2\frac{d_{ij}^2}{\hat{d}_{ij}^2}\right) d\boldsymbol{\theta}_1\cdots d\boldsymbol{\theta}_N}{\int_{S_N}\cdots\int_{S_1} \prod_{i=1}^{N}\prod_{j=i+1}^{N+M} \exp\left(-\frac{\alpha}{8}\ln^2\frac{d_{ij}^2}{\hat{d}_{ij}^2}\right) d\boldsymbol{\theta}_1\cdots d\boldsymbol{\theta}_N} \\ \hat{y}_{i,\mathrm{MMSE}} &= \frac{\int_{S_N}\cdots\int_{S_1} y_i \prod_{i=1}^{N}\prod_{j=i+1}^{N+M} \exp\left(-\frac{\alpha}{8}\ln^2\frac{d_{ij}^2}{\hat{d}_{ij}^2}\right) d\boldsymbol{\theta}_1\cdots d\boldsymbol{\theta}_N}{\int_{S_N}\cdots\int_{S_1} \prod_{i=1}^{N}\prod_{j=i+1}^{N+M} \exp\left(-\frac{\alpha}{8}\ln^2\frac{d_{ij}^2}{\hat{d}_{ij}^2}\right) d\boldsymbol{\theta}_1\cdots d\boldsymbol{\theta}_N} \end{aligned} \tag{5.11}$$

where ln is the natural logarithm and

$$\int \cdot\, d\boldsymbol{\theta}_i \equiv \int\int \cdot\, dx_i dy_i. \tag{5.12}$$

S_i is the integral region for $\boldsymbol{\theta}_i = (x_i, y_i)$, expressed as

$$S_i = \left\{ (x_i, y_i) \,\middle|\, \begin{array}{l} x_i \in (O_{ix} - A_i, O_{ix} + A_i) \\ y_i \in (O_{iy} - B_i, O_{iy} + B_i) \end{array} \right\}. \tag{5.13}$$

$$\alpha = \left(\frac{10n_p}{\sigma_{dB}\ln 10}\right)^2, \tag{5.14}$$

and

$$\hat{d}_{ij} = d_0 \left(\frac{P_0}{P_{ij}}\right)^{1/n_p}. \tag{5.15}$$

Obviously, $d_{ij}^2 = (x_i - x_j)^2 + (y_i - y_j)^2$. The notation $\hat{d}_{ij}$ is used for the expression in (5.15) because (5.15) can be interpreted as the maximum likelihood estimation for d_{ij} which maximizes the likelihood distribution $f(P_{ij}|d_{ij})$. When (5.11) is implemented

in actual wireless networks, P_{ij} is reported by the wireless nodes and (5.15) is used to compute $\hat{d}_{ij}$. For computer simulations, since P_{ij} contributes to MMSE cooperative position estimation (5.11) only through $\hat{d}_{ij}$, once (x_i, y_i), $i = 1, \cdots, N$ are randomly generated, $\hat{d}_{ij}$ can be obtained according to

$$\hat{d}_{ij} = d_{ij} 10^{\frac{\sigma_{dB}}{10n_p}G}. \tag{5.16}$$

where $G \sim \mathcal{N}(0,1)$ is a standard Gaussian random variable. See Appendix B.2 for derivation.

The expression (5.11) looks intimidating since it involves complicated multiple definite integrals which have no closed-form solutions. We are able to compute these integrals via numerical methods. One of the popular numerical methods for computing complicated definite integrals is the Simpon quadrature method [66]. However, Simpon quadrature function in Matlab can only deal with up to three fold multiple integral. Since each node has two parameters to be estimate, Simpon quadrature method is limited to the special case with $N = 1$, that is, single node positioning. For multiple nodes positioning ($N > 1$), Monte Carlo method [66] is adopted.

A non-cooperative version of the proposed MMSE estimator can be obtained by forcing $N = 1$ and applying the estimator (5.11) with $N = 1$ to each of the unknown nodes respectively while ignoring all other unknown nodes. That is, $(\hat{x}_i, \hat{y}_i)$ is simply based on P_{ij} with $j = N+1, \cdots, N+M$ (M anchor nodes). In this way, though the advantages of cooperative methods are lost, the estimator is still optimum in MSE sense among all non-cooperative estimators. Thus, the performance of some existing iterative positioning approaches, such as MLE, can be improved if the estimates achieved via non-cooperative version of the proposed algorithm are used as initial positions. An example is the MMSE-MLE mentioned above and to be presented later.

Table 5.1
Symbol Explanation for Figures 5.1~5.3

Symbol	Meaning
blue square	anchor nodes
red dot	the true position
blue asterisk	estimated position
black diamond	the mean of the estimated positions for a true position
black ellipse	uncertainty ellipse
red ellipse	CRB ellipse

5.4.3 Performance and Properties

Without loss of generality, from now on, we focus on the simplest special case of the a priori PDF (5.10) where all unknown nodes take position independently and uniformly within the same square area of unit length centered at $(1/2, 1/2)$, that is, $(O_{ix}, O_{iy}) = (1/2, 1/2)$ and $A_i = B_i = 1/2$ for any i. There is one anchor node at each of the four corners. This model is also employed in [40,63]. Actually, many practical situations, such as storage rooms, play grounds and offices, fit in this square model. Please note that all coordinates share the same unit, therefore it is unnecessary to assign a specific unit to the coordinates. Now, the MMSE estimator (5.11) is reduced to

$$\begin{aligned}
\hat{x}_{i,\mathrm{MMSE}} &= \frac{\int_S \cdots \int_S x_i \prod_{i=1}^{N} \prod_{j=i+1}^{N+M} \exp\left(-\frac{\alpha}{8} \ln^2 \frac{d_{ij}^2}{\hat{d}_{ij}^2}\right) d\boldsymbol{\theta}_1 \cdots d\boldsymbol{\theta}_N}{\int_S \cdots \int_S \prod_{i=1}^{N} \prod_{j=i+1}^{N+M} \exp\left(-\frac{\alpha}{8} \ln^2 \frac{d_{ij}^2}{\hat{d}_{ij}^2}\right) d\boldsymbol{\theta}_1 \cdots d\boldsymbol{\theta}_N} \\
\hat{y}_{i,\mathrm{MMSE}} &= \frac{\int_S \cdots \int_S y_i \prod_{i=1}^{N} \prod_{j=i+1}^{N+M} \exp\left(-\frac{\alpha}{8} \ln^2 \frac{d_{ij}^2}{\hat{d}_{ij}^2}\right) d\boldsymbol{\theta}_1 \cdots d\boldsymbol{\theta}_N}{\int_S \cdots \int_S \prod_{i=1}^{N} \prod_{j=i+1}^{N+M} \exp\left(-\frac{\alpha}{8} \ln^2 \frac{d_{ij}^2}{\hat{d}_{ij}^2}\right) d\boldsymbol{\theta}_1 \cdots d\boldsymbol{\theta}_N}
\end{aligned} \tag{5.17}$$

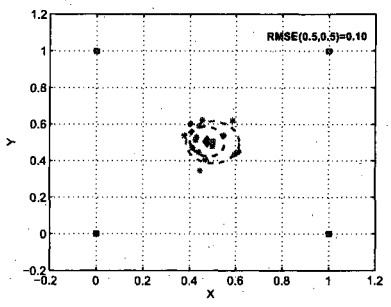

(a) Center Position $(\tilde{x}, \tilde{y}) = (0.5, 0.5)$

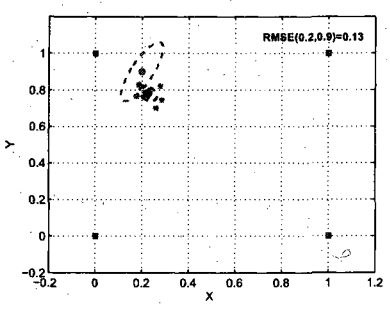

(b) Corner Position $(\tilde{x}, \tilde{y}) = (0.2, 0.9)$

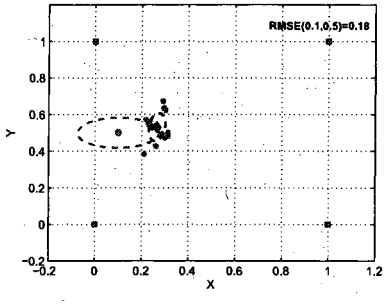

(c) Side Position $(\tilde{x}, \tilde{y}) = (0.1, 0.5)$

Figure 5.1. MMSE estimator for different true positions. See Table 5.1 for symbol explanations.

for any i from 1 to N, where α and $\hat{d}_{ij}$ are expressed in (5.14) and (5.15) respectively, and

$$S = \{(x_i, y_i) | 0 \leq x_i \leq 1, 0 \leq y_i \leq 1\}.$$

Since MSE has the meaning of average squared distance error, to indicate the average distance error instead, the root mean squared error (RMSE), defined as RMSE $= \sqrt{\text{MSE}}$, is often used in practice as a measure for goodness of the estimator. To gain more insights into the behavior of the proposed MMSE estimator, we also study how different true positions contribute differently to the average MSE.

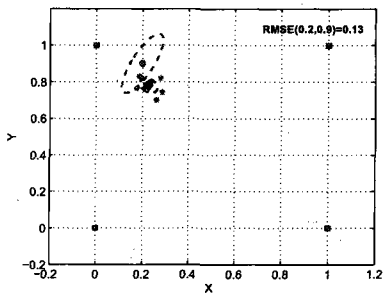

(a) MMSE

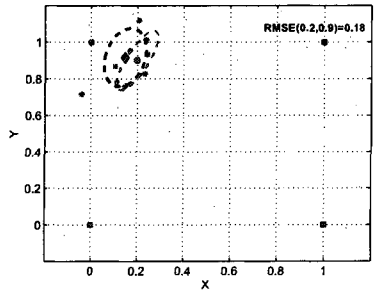

(b) MLE (with random initial estimation)

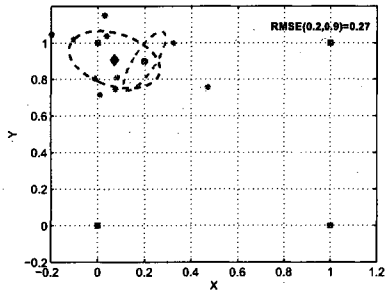

(c) MDS

Figure 5.2. Comparison of MMSE, MLE and MDS position estimators for the side position $(\tilde{x}, \tilde{y}) = (0.2, 0.9)$. See Table 5.1 for symbol explanations.

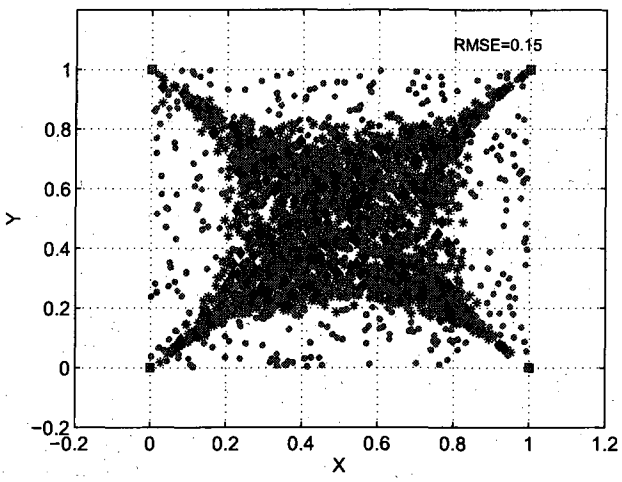

Figure 5.3. MMSE cooperative position estimator. See Table 5.1 for symbol explanations.

This property can be characterized by RMSE$(\tilde{x}, \tilde{y})$, the RMSE for a particular true position $(\tilde{x}, \tilde{y})$, which is expressed as

$$\text{RMSE}(\tilde{x}, \tilde{y}) = \sqrt{\mathsf{E}[(\tilde{x} - \hat{\tilde{x}})^2 + (\tilde{y} - \hat{\tilde{y}})^2 | (\tilde{x}, \tilde{y})]}, \tag{5.18}$$

where the expectation is taken only with respect to $(\hat{\tilde{x}}, \hat{\tilde{y}})$.

While RMSE measures the overall performance of an estimator, the standard deviation, the square root of the variance, is also of interest since it tells the "stability" of an estimator. In practical positioning applications, the wireless channel usually does not change fast enough for one to obtain different observations, thus taking the mean of different estimated positions as the final estimate is not quite practical. Under such circumstances, among estimators that achieve approximately the same RMSE, an estimator with a smaller standard deviation is more desirable. For unbiased estimators, the RMSE equals the standard deviation. And the well known Cramér-Rao bound (CRB) expresses a lower bound on the standard deviation or the RMSE of unbiased estimators. Detailed derivation for CRB expression for position estimators can be found in [49].

Figures 5.1, 5.2 and 5.3 to be presented in the following illustrate the properties of the proposed MMSE estimator. The symbols used in these figures are summarized in Table 5.1.

In Figure5.1, the performance of the MMSE estimator for different true positions is illustrated. A position close to the a priori center, near a corner and besides a side are called a *center position*, a *corner position* and a *side position*, respectively. We study RMSE$(\tilde{x}, \tilde{y})$ for these three different types of positions via simulations. As an example, in Figure5.1, three positions are picked at the a priori center $(0.5, 0.5)$, near the corner $(0.2, 0.9)$ and near a side $(0.1, 0.5)$.

Firstly, as shown in Figure5.1, RMSE of the MMSE estimator is smaller than the CRB, the lower bound on the RMSE of all unbiased estimator. This is generally true for any N as verified by the simulation results shown later. Since the existing popular position estimators, such as MLE and MDS, can only achieve near-CRB performance, the CRB is virtually considered as a limit for the performance of a positioning estimator. With the proposed MMSE estimator, CRB is not an unreachable limit any longer. It is also seen that the uncertainty ellipse (black dashed ellipse) is quite small, even smaller than CRB ellipse (red dashed ellipse). This indicates that MMSE estimator is quite stable, which makes the MMSE positioning algorithm more attractive. It is obvious that MMSE is a biased estimator, but it achieves a delicate trade-off between the bias and the variance and obtain position estimates even better than the CRB.

It is also shown in Figure5.1 that the RMSE for the center positions is smaller than that for those positions further away from the a priori center. This is expected since MMSE generally works better when true value gets closer to the expectation [48]. Furthermore, among the positions far away from the a priori center, the RMSE for corner positions is smaller than that for side positions. Intuitive explanations are the MMSE estimator for a corner position is inherently restricted into a smaller area than that for a side position and is thus subject to smaller possible errors.

The MMSE estimator is compared with MLE and MDS for the same corner position $(\tilde{x}, \tilde{y}) = (0.2, 0.9)$ in Figure 5.2, where Figure 5.1(b) is the same as Figure 5.1(b) and copied here for convenience. An obvious and significant difference of MMSE estimator from MLE and MDS is that MMSE estimated positions always fall within the possible range for the unknown position, however MLE or MDS estimated positions are very likely to violate the possible position range. In other words, MMSE estimated positions are always valid for the given restrictions on the positions, while MLE or MDS estimated positions are not guaranteed to be valid and thus sometimes are apparently ridiculous. Actually, the fact that MMSE estimated value can never be out of range can be easily proved using the general formula (5.6), and such a property of MMSE estimator partially explains why MSE of MMSE estimator is smaller than other estimators. Please note that though for the example $(\tilde{x}, \tilde{y}) = (0.2, 0.9)$, RMSE$(\tilde{x}, \tilde{y})$ of MMSE is smaller than that of MLE and MDS, we are not trying to say that RMSE$(\tilde{x}, \tilde{y})$ of MMSE is the smallest for any $(\tilde{x}, \tilde{y})$. Actually, for true positions near the center, RMSE of MMSE is smaller than that of MLE, but for true positions away from the center, RMSE of MMSE is bigger than that of MLE. MMSE achieves the minimum MSE in an average sense. In terms of the standard deviation, the MLE and MDS are obviously worse than CRB and much worse than MMSE.

To have a complete picture about how the MMSE estimator performs, 500 positions are randomly picked as the true positions for $N = 1$ case and the result is shown in Figure 5.3, where as before, each true position is represented by a red dot and different estimated positions for each true position are shown as blue asterisk and their means are shown as black diamonds. It is noticed that though the true positions are uniformly distributed among the whole square, the estimated positions tend to fall within a squeezed-box shape area as covered by the blue or the black diamonds. This means that the bias of MMSE estimator is much larger for those side positions. This observation motivates two variations of the MMSE estimator, MMSE-MAP and MMSE-Double, which will be presented in the next section (Section 5.5.2).

5.5 Variations of MMSE Cooperative Positioning Algorithms

Based on studies on the proposed MMSE cooperative positioning algorithm in the previous section, we proposed in this section three variations of the original MMSE estimator.

5.5.1 MMSE-Big

According to the section 5.4.3, better RMSE is achieved by the original MMSE estimator for nodes that are closer to the a priori center. This enlightened the thought that if we could "push" all nodes closer to the center then the overall performance may be improved. Since the a priori PDF for the true positions (named *actual a priori PDF*) is fixed, we can not actually push the nodes for them to be closer to the center. However, we can consider a larger square for the a priori PDF used for computing the conditional mean (named *virtual a priori PDF*). This equivalently brings all nodes appear relatively closer to the center. Specifically, as sketched in Figure 5.4, though the true position (x, y) is distributed according to uniform distribution within an 1 by 1 square (solid line), the uniform distribution within a larger $1 + 2d$ by $1 + 2d$ square (dashed line) is used instead for computing integrals for the conditional mean. The resulting MMSE estimator is named *MMSE-Big* estimator, which is obtained according to (5.11) with

$$S_i = \{(x_i, y_i) | -d \leq x_i \leq 1 + d, -d \leq y_i \leq 1 + d\}, \forall i.$$

An empirical value for d is one quarter of the side length. In our case, $d = 0.1$. MMSE-Big improves the RMSE performance (as shown by the simulation results later) without any extra computation burden. It is noted that in the original MMSE estimator, the actual a priori PDF is the same as the virtual a priori PDF.

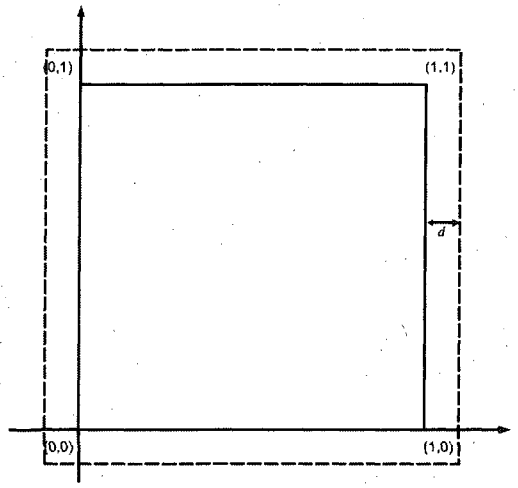

Figure 5.4. MMSE-Big estimator uses the larger square (dashed line) for the virtual a priori PDF, while the smaller square (solid line) is for the actual a priori PDF.

5.5.2 MMSE-Mapping and MMSE-Double

Figure5.3 in the section 5.4.3 revealed that though the true positions are scattered all over the whole square area, the positions estimated by the original MMSE estimator fall within a squeezed-box shape area. Based on this observation, we proposed to map the MMSE estimated position to a new position so that the area covered by the estimated positions after mapping can overlap with the area covered by the true positions as much as possible. Intuitively, this would bring the mean estimated positions closer to the true position and thus reduce the bias and the RMSE. The obtained estimator is named MMSE-Mapping.

The mapping is illustrated in Figure 5.5, where the square, the original area where all nodes appear, is divided into four regions marked by 1 to 4, and the circumcircle is introduced for mapping. P at $(\hat{x}, \hat{y})$ is the original MMSE estimated position and P^* at $(\hat{x}^*, \hat{y}^*)$ is the new estimated position after mapping. An auxiliary line, connecting

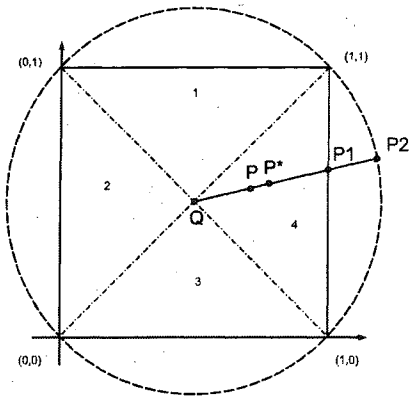

Figure 5.5. Proposed mapping.

the center point Q at $(1/2, 1/2)$ and P, intersects the square at P_1 and the circumcircle at P_2. We choose P^* so that

$$\frac{d(P^*, Q)}{d(P, Q)} = \frac{d(P_2, Q)}{d(P_1, Q)}, \tag{5.19}$$

where $d(A, B)$ stands for the distance between the point A and the point B. Obviously, $d(P_2, Q) = \sqrt{2}/2$, the radius of the circumcircle. Let k be the slope of the auxiliary line, thus $k = \frac{\hat{y}-\frac{1}{2}}{\hat{x}-\frac{1}{2}}$. The coordinates of P_1, (x_{P_1}, y_{P_1}), which are needed to compute $d(P_1, Q)$, are

$$(x_{P_1}, y_{P_1}) = \begin{cases} (\frac{1}{2} + \frac{1}{2k}, 1) & \text{if } P_1 \text{ is in the region 1} \\ (0, \frac{1}{2} - \frac{k}{2}) & \text{if } P_1 \text{ is in the region 2} \\ (1, \frac{1}{2} + \frac{k}{2}) & \text{if } P_1 \text{ is in the region 3} \\ (\frac{1}{2} - \frac{1}{2k}, 0) & \text{if } P_1 \text{ is in the region 4} \end{cases}. \tag{5.20}$$

According to the mapping rule in (5.19), it is easy to derive that

$$\begin{cases} \hat{x}^* = \frac{1}{2} + \frac{\sqrt{2}}{2} \frac{d(P,Q)}{d(P_1,Q)} \cos\theta \\ \hat{y}^* = \frac{1}{2} + \frac{\sqrt{2}}{2} \frac{d(P,Q)}{d(P_1,Q)} \sin\theta \end{cases} \tag{5.21}$$

where, $d(P, Q) = \sqrt{(\hat{x} - 1/2)^2 + (\hat{y} - 1/2)^2}$, $d(P_1, Q) = \sqrt{(x_{P_1} - 1/2)^2 + (y_{P_1} - 1/2)^2}$ with (x_{P_1}, y_{P_1}) obtained according to (5.20), and $\theta = \arg\tan \frac{\hat{y}-\frac{1}{2}}{\hat{x}-\frac{1}{2}}$, which is the angle of the auxiliary line.

Performance can be further improved if we apply the MMSE estimation method again, assuming that each true position is uniformly distributed within a new smaller square whose center is the corresponding MMSE-Mapping estimator, i.e. the estimated position after mapping. Empirically, the length of the smaller square can be chose as one fifth of the length of the original square. The obtained new estimator is named MMSE-Double, since we apply MMSE twice. To put it precisely, the MMSE-Double estimator is obtained using (5.11), where $A_i = B_i = 0.2$ and $(O_{ix}, O_{iy}) = (\hat{x}_i^*, \hat{y}_i^*)$ with $(\hat{x}_i^*, \hat{y}_i^*)$ being obtained according to (5.21) (the mapping step) from the original MMSE estimator $(\hat{x}_i, \hat{y}_i)$. The MMSE-Double works like a turbo engine. After the first time MMSE is implemented, mapping is carried out to tune up the estimated positions. These new estimated positions are used to determine the centers of smaller square areas so that MMSE can be implemented again with the new virtual a priori PDF.

5.5.3 MMSE-MLE

The well known MLE positioning estimator, which is solved iteratively, is quite sensitive to the initial estimation. On one hand, it is a disaster if the initial estimation is randomly generated as shown in Figure 5.6(a) ; on the other hand, if the perfect initial estimation, i.e. the true position, is used, MLE works extremely well as shown in Figure 5.6(b). True positions are unknown and to be estimated, so MLE with perfect initial estimation is an ideal and impractical situation. Fortunately, a very good initial estimation can be obtained quickly by applying the proposed MMSE algorithm to each of the nodes respectively in a non-cooperative fashion, as mentioned in the section 5.4.2. The obtained MMSE initial estimation is then fed into the iterative algorithm for MLE. The resulting estimator is then named MMSE-MLE. To improve the accuracy of initial estimator, we can implement certain variation of MMSE, such as MMSE-Big (Section 5.5.1), instead of the original MMSE. The performance of MMSE-MLE using MMSE-Big is shown in Figure 5.6(c). It can

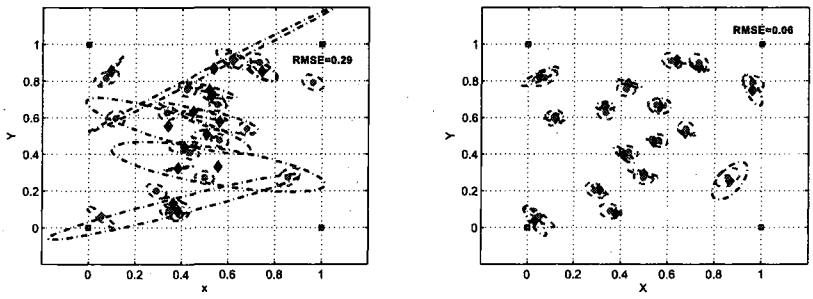

(a) MLE with Random Initial Estima- (b) MLE with Perfect Initial Estimation
tion

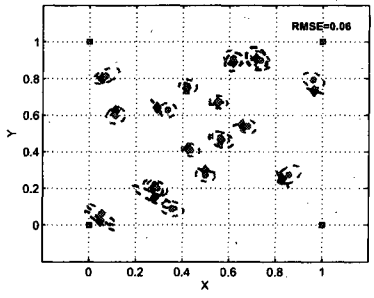

(c) MLE with MMSE-Big Initial Estimation (MMSE-MLE)

Figure 5.6. MMSE-MLE performs as well as MLE with perfect initial estimation ($N = 20$). Same symbols as given in Table 5.1 are used.

be seen that MMSE-MLE performs as well as MLE with perfect initial estimation. In [62], we also proposed to use MDS estimator as the initial estimation for MLE (MDS-MLE). Since MDS is inferior to MMSE, it can be expected that MDS-MLE works worse than MMSE-MLE as verified by the simulation results shown in the next section.

Compared with MMSE, MMSE-MLE requires less computation at the cost of worse MSE performance. It is observed that the performance advantage of MMSE over other estimators diminishes fast as the size of the network N increases. Therefore, MMSE-MLE is preferable for large size networks, considering that the benefits of

MMSE are not worth its huge computation burden, and MMSE-MLE is able to achieve near CRB performance. For small size networks, the computation speed difference between MMSE and MMSE-MLE is not too much, thus MMSE is chosen for purpose of better performance.

As a summary, we compare all MMSE and its variations with existing popular algorithms MLE, MDS in terms of the standard deviation (STD) and the RMSE. The results for $N = 1$ are listed in Tab. 5.2 where "MLE" refers to the regular MLE with random initial estimation and "MLE-Ideal" refers to the MLE algorithm with the true positions as the perfect initial estimation, which is the ideal case for MLE. The CRB is also provided for comparison. For unbiased estimators, RMSE and STD are equal and thus sometimes are not discriminated in some works. However, RMSE and STD represent different meanings and are different for biased estimators. For positioning problems, while RMSE reflects the average distance error between the true and the estimated positions, STD shows how stable an estimator can be. For overall evaluation of estimator performance, RMSE is more significant than STD. The STD of MLE-Ideal is close to CRB, the lower bound for STD of unbiased estimators. In the sense of RMSE, since MMSE is better than CRB, MMSE are better than any unbiased estimator.

5.6 Numerical Results and Analysis

In Figure5.7 and Figure 5.8, the RMSE and the standard deviation for $N = 5 \sim 7$ are respectively shown for the proposed MMSE cooperative estimator (MMSE), its variation MMSE-Big, MDS, MLE with random initial estimation (MLE), MLE with MDS used as the initial estimation (MDS-MLE). CRB is also provided. It can be seen that MMSE-Big brings obvious performance improvement over MMSE for any N and they both are better than the CRB.

Roughly speaking, the power degradation between two nodes are inversely proportional to the distance between them. While the MMSE and MLE are based on

Table 5.2
Comparison of Different Estimators

Estimator	RMSE	STD
MDS	0.2571	0.2505
MLE	0.2031	0.1989
MDS-MLE	0.1959	0.192
MLE-Ideal	0.1928	0.188
CRB=0.1811		
MMSE	0.1515	0.0832
MMSE-Mapping	0.142	0.1271
MMSE-Big	0.1344	0.0965
MMSE-Double	0.1329	0.1115

MLE : MLE with random initial estimation

MLE-Ideal : MLE with true positions as initial estimation

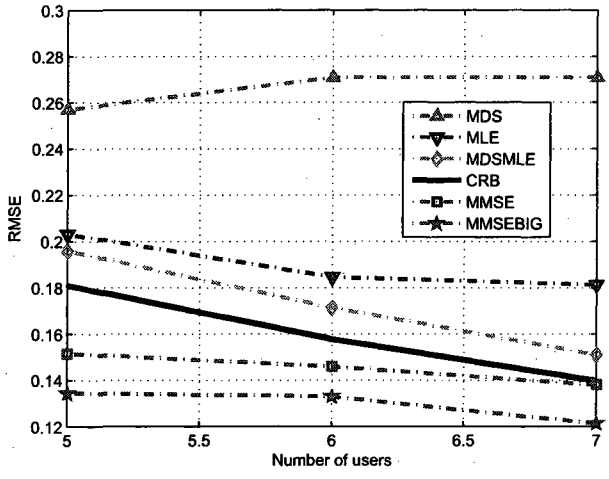

Figure 5.7. RMSE of different algorithms.

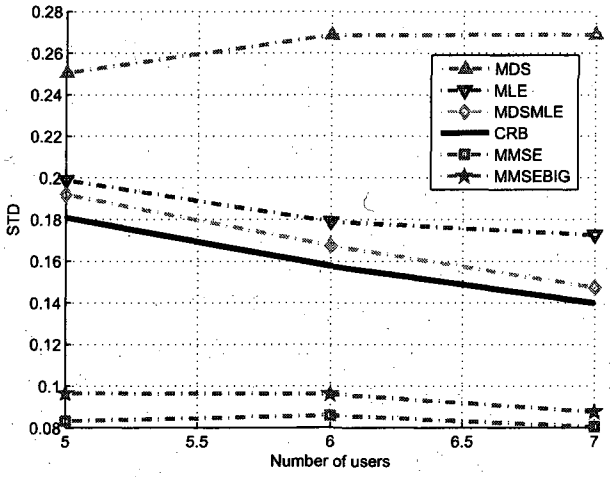

Figure 5.8. STD of different algorithms.

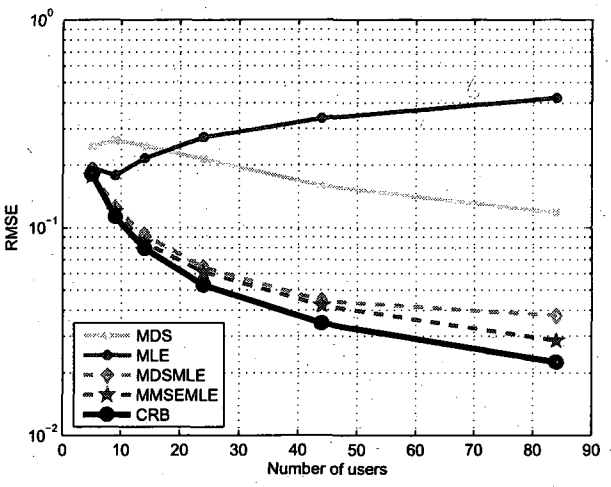

Figure 5.9. RMSE of different algorithms for large size networks.

the power degradation and thus incur small errors for small distance, MDS is based on the distance and brings larger error to small distance. This reveals the underlying reason for the bad performance of MDS.

For wireless networks of large size, we can partition the whole group of nodes into smaller group and apply our MMSE estimator without losing much performance compared to applying MMSE to the whole large size network. Another solution for large size network is MMSE-MLE, which sacrifices performance for computation complexity. As shown in Figure 5.9, MMSE-MLE achieves near CRB performance, which is the best performance MLE can achieve for any possible initial estimation.

5.7 Conclusions and Future Work

For the sake of application of Bayesian estimation in wireless networks in cooperative way, it is obligated to find a simple way to calculate the multidimensional integration of Bayesian MMSE. This is a our future work for MMSE.

To the best of our knowledge, this chapter is the first to present an outline of MMSE estimation for nodes cooperative positioning in wireless network . Starting from a channel verified by real measurement, this chapter addresses a complete derivation for MMSE estimation and other variation versions. Armed with those theoretical analysis and equations, we find some numerical solutions to realize MMSE. Furthermore, from this chapter, we may acquire a thorough point of view for MDS,MLE, MAP, MMSE and CR-bound for node cooperative positioning in wireless network. Considering the preeminent performance of MMSE, MMSE must have been taking up more and more share for nodes cooperative positioning in wireless network applications.

CHAPTER 6

ITERATIVE COOPERATIVE POSITIONING ALGORITHM IN WIRELESS NETWORKS

6.1 Introduction

From the previous chapter, it is known that MMSE cooperative positioning algorithm has distinct advantages over the classical positioning algorithms such as MDS or MLE. However, it is not practical to apply MMSE cooperative positioning to networks of a large number of unknown nodes due to high computation burden of calculating the multiple integrals present in its formulas Eq. (5.11). In this chapter, we propose an adaptive iterative cooperative (AIC) positioning algorithm, which enables us to efficiently get an approximate solution to the exact MMSE position estimator. The accuracy is almost the same as that of the results obtained by directly calculating the multiple integrals via numerical methods, while the computation cost is highly decreased so that the proposed method is practical for applications in real world.

After the detailed scheme of MMSE-AIC is presented, the performance analysis and numerical results are also provided in this chapter. Finally, all of the positioning algorithms studied in previous three chapters are put together and compared side-by-side.

This chapter is organized as follows. The system model is described in the section 6.2. In the section 6.3, the proposed MMSE-AIC cooperative positioning algorithm is described in detail. The superior performance of the proposed MMSE-AIC estimator is further verified by the numerical results with some analysis presented in the section 6.4. Overall comparison of all positioning algorithms is presented in the section 6.5. Conclusion of this chapter is addressed in the section 6.6.

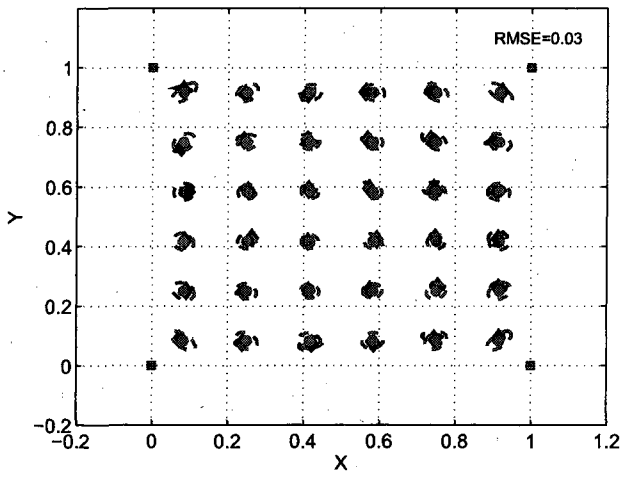

Figure 6.1. Uniform fixed distribution for $N = 36$ unknown nodes.

6.2 System Model

The system model given in previous two chapters is also adopted in this chapter with only one difference, which is the distribution of unknown nodes. In previous chapters, a random distribution of unknown nodes are consided. In this chapter, given the number of unknown nodes, they take positions uniformly within the considered area. Unlike in chapter 5 where the number of unknown nodes is small, in this chapter we are dealing with large size wireless networks, where it is not practical and not necessary to evaluate the performance using random distribution. Therefore as in most of current works, we evaluate our estimator using uniformly distributed unknown nodes.

The uniform distribution for 36 unknown nodes, as well as the anchor nodes, is illustrated in Figure 6.1, where the unknown nodes are red diamonds. The complete explanation for different symbols has been given in Tab. 5.1.

Last but not least, we would like to point out that we do not have to acquire all pair-wise measurements for our system model. In other words, our cooperative

positioning algorithm can work well with partial pair-wise measurements hardly at any cost of accuracy.

6.3 Adaptive Iterative MMSE Cooperative Positioning

The proposed MMSE-AIC algorithm is carried out as follow. Firstly, the unknown node position is estimated solely based on the anchor nodes. Secondly, for each of the unknown nodes, we re-estimate its position assuming that all other unknown nodes are anchor nodes. This step should be carried out for all unknown nodes. This second step, which applies from the first to the last unknown nodes, is repeated iteratively until convergence when RMSE stops decreasing.

One of our important findings is that the number of needed iteration can be determined as a function of the number of unknown nodes. Suppose the number of unknown nodes is N. Empirically, the iteration number is $3\sqrt{N}$. For example, when $N = 25$, $3\sqrt{25} \approx 15$ iterations need to be run before convergence.

As defined previously, for MMSE estimation, a virtual a priori PDF is assumed for the possible area within which an unknown node may appear. And we assume uniform random distribution within a square as this virtual a priori PDF. During the iteration, the size of this square, or the edge length of the square, is not fixed but adaptively changed as the iterations proceed. This is why our algorithm is an adaptive method. The edge length of the square is referred to as *step size* for our iterative algorithm. How to select iterative step size for different iterations is crucial to our algorithm. And it is a very delicate job. If choosing a big area for next iteration of estimation, we speed up the iteration but lose the accuracy. And if small area is used, the convergence speed is slowed down and higher accuracy is not guaranteed to be achieved either. The empirical step size is the reciprocal of iteration numbers for the first several iterations and keeps the reciprocal of root square of number of unknown nodes, i.e. $1/\sqrt{N}$, for the remaining iterations. Take the previous example

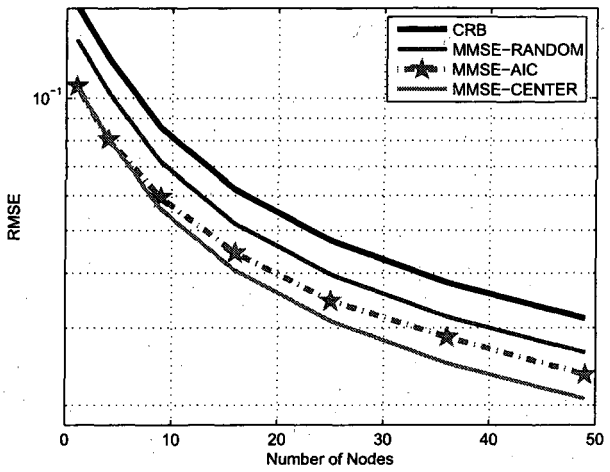

Figure 6.2. The bound of MMSE-AIC positioning.

of $N = 25$. The step sizes from the first iteration are 1/1,1/2,1/3,1/4,1/5,1/5... of one unit.

6.4 Numerical Results and Analysis

We propose two standards to evaluate the performance of MMSE-AIC: MMSE upper bound obtained using random distribution (MMSE-Random) and MMSE lower bound obtained using center unknown nodes (MMSE-Center). The bounds are shown in Figure6.2. For the case of single unknown node, the starting point of the MMSE-Random is obtained as the worst case for MMSE (random distribution) and the starting point of the MMSE-Center is obtained as the best case (center position). Then each of the two curves is extended to the case of more nodes by multiplying the CRB curve by the MMSE-over-CRB ratio corresponding to single unknown node.

In Figure6.3, we can see that RMSE is decreasing with more iterations. At each iteration, the RMSE does not keep decreasing as the number of nodes increases. This is because MMSE based algorithm is sensitive to the position of unknown nodes, which is the essential characteristics of MMSE estimators.

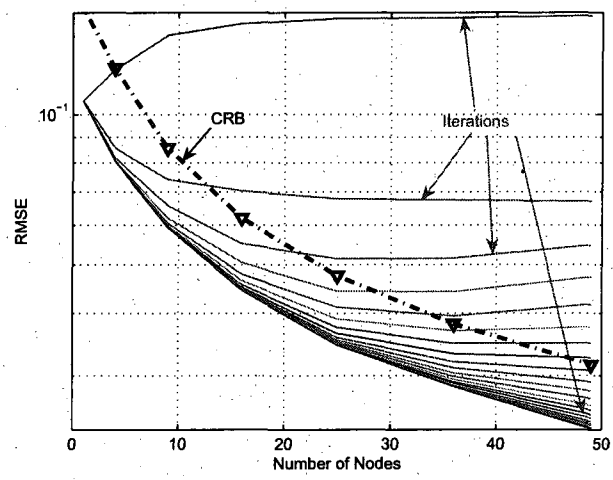

Figure 6.3. RMSE of MMSE-AIC positioning algorithm at different iterations.

6.5 Overall Comparison of Different Positioning Algorithms

As mentioned in the section 6.2, for large size networks, the uniform fixed distribution should be used if we want to make a fair comparison among all algorithms. Illustration of estimated positions for the same group of uniform distributed unknown nodes using different algorithms is shown in Fig 6.4. Their RMSE performance is presented in Figure6.5.

Based on Figure6.5, we can reach the conclusions about how well different algorithms work in terms of complexity and RMSE, as listed in the following Tab. 6.1.

6.6 Conclusions

In this chapter, we provide a pratical solution for MMSE cooperative positioning. The numerical results verifies that, according to RMSE criterion, MMSE-AIC outperforms any other cooperative positioning algorithms, such as MDS and MLE, and it beats the original solution to MMSE, which directly calculates multiple integrals, in terms of complexity. Moreover, it is a good example to enlighten us how to solve the

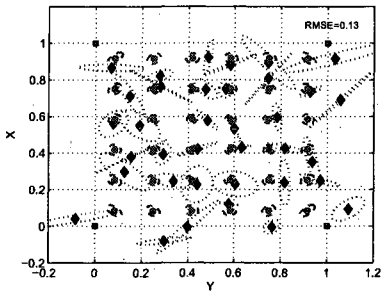

(a) MDS

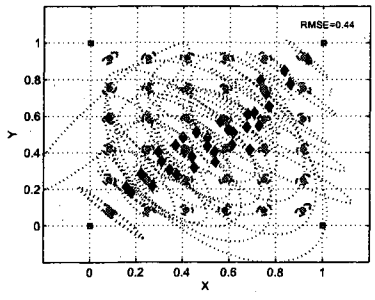

(b) MLE with Random Initial Estimation (MLE)

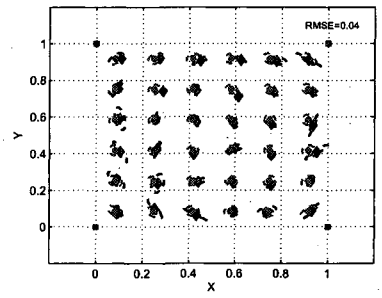

(c) MLE with Perfect Initial Estimation (MLE-IDEAL)

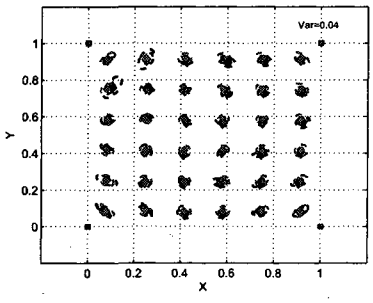

(d) MLE with MDS Initial Estimation (MDS-MLE)

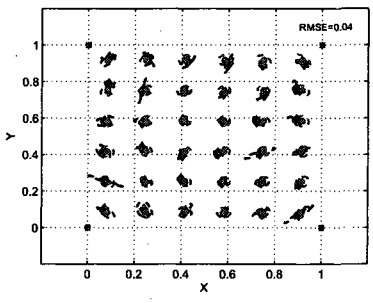

(e) MLE with MMSE-Big Initial Estimation (MMSE-MLE)

Figure 6.4. All positioning algorithms are presented here. Same symbols as given in Table 5.1 are used.

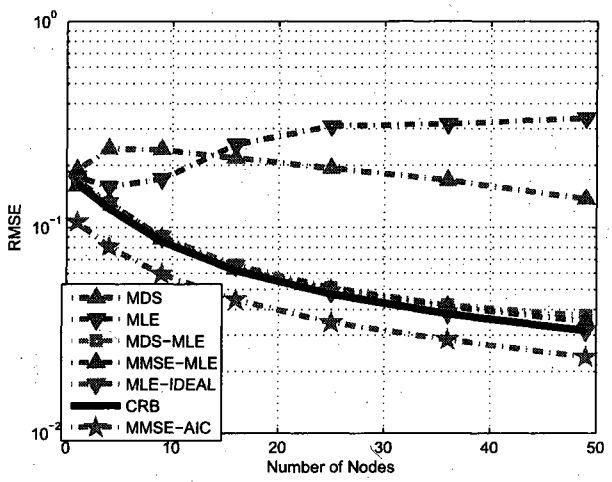

Figure 6.5. RMSE performance of different positioning algorithms.

Table 6.1
Overall Comparison of Different Positioning Algorithms

Algorithm	Complexity	RMSE
MDS	low	acceptable
MLE	medium	very poor
MDS-MLE	low medium	good
MMSE-MLE	medium	better
MLE-Ideal	low medium	better
MMSE-AIC	upper medium	best

intimidating mathematical multiple integrals and obtain perfect engineering results in practice.

CHAPTER 7

SUMMARY

7.1 Primary Contributions

The contributions accomplished by our work presented in this dissertation can be summarized as follows:

1. *Turbo equalization with Alamounti codes working in frequency domain:* We are the first research team to propose and study this scheme that applies turbo equalization in frequency domain and integrates it with Alamounti codes based on multiple (usually two) antennas. Most other similar research works focus on the time domain and single antenna. On one hand, frequency domain turbo equalization we proposed can be used for single carrier and combat inter-symbol-interference (ISI) better than the time domain equalization. On the other hand, adoption of antenna array for Alamounti code brings further performance enhancement over single antenna system.

2. *A new channel capacity bound for MISO cooperative communications:* The channel capacity bound for MIMO cooperative communications is a well recognized world-wide difficult problem. So far, no one, including some famous professors, can provide a complete solution for this problem. We start with a simpler but crucial problem, that is, the capacity bound for MISO cooperative communications. To explore this problem is one of the unavoidable steps on the way to solve the final problem of MIMO cooperative communications. We derive our own capacity outer bound for MISO cooperative communications. We are very glad to make some contribution to solve that world-wide difficult problem even though we can not obtain the complete solutions.

3. *An improved classical positioning algorithm MDS-MLE to be implemented on a Zig-bee hardware platform:* MLE is an existing classical positioning method proposed by a prestigious research team, however we find that there is a problem with initialization of the original algorithm. Through the independent research and hard work, we propose to combine another classical positioning algorithm MDS with MLE to fix the problem. Furthermore, we built a real wireless system using Zig-bee devices and implement the proposed MDS-MLE positioning algorithm on this platform. We chose Zig-bee devices because it is suitable for our positioning algorithm due to many of its own features, such as low-cost, flexible applications. No one else has ever used Zig-bee system for indoor positioning.

4. *An MMSE positioning algorithm that can break through the CR bound :* The CR bound is the final frontier for classical positioning algorithm. There are a large number of published papers where new ideas, schemes or algorithms are proposed simply to get close to the CR bound. In our work, we propose and derive an MMSE algorithm, which is a new positioning algorithm based on the Bayesian theory. The proposed MMSE positioning algorithm breaks through the CR bound, which can be proved theoretically and verified by simulation results. An issue with the proposed MMSE algorithm is that the computation burden for calculating multiple integrals via numerical methods gets unaffordable when the number of unknown nodes is very large. This motivates our next step which is to find the a practical solution for MMSE algorithm.

5. *A practical solution for MMSE algorithm:* As mentioned in the item 4, we need to a practical solution for MMSE algorithm, that is, to find a computation efficient method to obtain MMSE estimated positions. With this motivation, we make further study on MMSE and propose the innovative MMSE Adaptive Iterative Cooperative (AIC) method, which works iteratively as a turbo engine without losing much accuracy. Without any exaggeration, this MMSE-AIC is the best positioning algorithm among existing positioning algorithm in term of RMSE.

7.2 Future Work

For each of the topics mentioned above, there is still some work left to be done in the future:

1. *Turbo equalization with Alamounti codes working in frequency domain:* Although simulations have proved this scheme is better than others, there is a small gap between the simulation results and theory. Our future work on this topic is to do more research work to prove the gap is caused by the simulation system error.

2. *A new channel capacity bound for MISO cooperative communications:* We have just obtained the outer capacity bound for MISO cooperative communications. It is still a long way to fulfill our final target that is to derive the channel capacity bound for MIMO cooperative communications.

3. *An improved classical positioning algorithm MDS-MLE to be implemented on a Zig-bee hardware platform:* We should try to use other wireless system platforms than Zig-bee system or explore some new features of Zig-bee wireless system platform to be exploited by the positioning algorithm. We should keep an eye on the development of wireless hardware maturefacured by various factories to seek suitable platforms for positioning algorithm .

4. *An MMSE positioning algorithm that can break through the CR bound :* Though closed-form expression for MMSE position estimator is an impossible mission today, we never give up the hope that, using more advanced mathematics , it is possible to obtain the close-form expression, or at least, to obtain certain approximate close-form expressions, for MMSE positioning algorithm. Our future work is to explore newly developed mathematics theory and tools to solve the multiple integrals problem existing in MMSE positioning algorithm.

5. *A practical solution for MMSE algorithm:* Through simulation and logic analysis, we provide the upper and lower bound for this practical solution. In the future, we should do more mathematic work to derive stricter upper and lower bounds.

Appendix A

Outline of Proof for Theorem 1

The paper [30] gives an outer bound on the capacity region of general single antenna partially cooperative RBC in terms of R_0, R_1, R_2. Examination of its proof reveals that it is straightforward to extend this theorem to the general MISO CBC. As mentioned before, I am only interested in the private messages, that is $R_0 = 0$. Hence, I can conclude that the capacity region of a general MISO CBC is outer bounded by the region with (R_1, R_2) that satisfies

$$\begin{aligned} R_1 < &\ \min\{I(U'; Y_1|X_1), I(\mathbf{X}; Y_1, Y_2|U, X_1)\} \\ R_2 < &\ \min\{I(U, X_1; Y_2), I(U; Y_1, Y_2|X_1), I(\mathbf{X}; Y_1, Y_2|U', X_1)\} \end{aligned} \tag{A.1}$$

for some joint distribution $p(u, u', x_1, \mathbf{x})p(y_1, y_2, |\mathbf{x}, x_1)$ that satisfies two Markov chain conditions: $X_1 \rightarrow U \rightarrow \mathbf{X}$ and $X_1 \rightarrow U' \rightarrow \mathbf{X}$. The auxiliary random variables U and U' are bounded in cardinality by $|\mathcal{U}| \leq |\boldsymbol{\mathcal{X}}| \cdot |\mathcal{X}| + 2$ and $|\mathcal{U}'| \leq |\boldsymbol{\mathcal{X}}| \cdot |\mathcal{X}| + 2$, respectively.

In the following, I present the derivation of (3.2) (Theorem 1) by specializing (A.1) to AWGN channel for any given channel realization.

I derive the expression for the capacity outer bound region for any fixed $\mathbf{Q}_\mathbf{X}$ and $\mathbf{q}_{\mathbf{X}X_1}$. The union of the obtained regions over all valid $\mathbf{Q}_\mathbf{X}$ and $\mathbf{q}_{\mathbf{X}X_1}$ gives us the entire outer bound as given in Theorem 1 (3.2).

A.1 Proof of outer bound for R_1 in Theorem 1

Let us start with $I(\mathbf{X}; Y_1, Y_2|U, X_1)$, where

$$\begin{aligned} I(\mathbf{X}; Y_1, Y_2|U, X_1) &= \mathsf{h}(Y_1, Y_2|U, X_1) - \mathsf{h}(Y_1, Y_2|\mathbf{X}, U, X_1) \\ &\overset{(1a)}{=} \mathsf{h}(Y_1, Y_2|U, X_1) - \mathsf{h}(Y_1, Y_2|\mathbf{X}, X_1) \\ &\leq \mathsf{h}(Y_1, Y_2|X_1) - \mathsf{h}(Y_1, Y_2|\mathbf{X}, X_1) \\ &= I(\mathbf{X}; Y_1, Y_2|X_1), \end{aligned} \tag{A.2}$$

where $(1a)$ follows from the fact that conditioned on $(X_1, \mathbf{X})$, (Y_1, Y_2) is independent of U. Thus, the bound for R_1 in (A.1) becomes

$$R_1 < \min\{I(U'; Y_1|X_1), I(\mathbf{X}; Y_1, Y_2|X_1)\}. \tag{A.3}$$

Although the specific expression for the maximal $I(\mathbf{X}; Y_1, Y_2|X_1)$ can be obtained as shown later, it is not necessary here. In fact,

$$\begin{aligned} I(\mathbf{X}; Y_1, Y_2|X_1) - I(U'; Y_1|X_1) &= \mathsf{h}(Y_1, Y_2|X_1) - \mathsf{h}(Y_1, Y_2|\mathbf{X}, X_1) - (\mathsf{h}(Y_1|X_1) - \mathsf{h}(Y_1|U', X_1)) \\ &= \mathsf{h}(Y_1|X_1) + \mathsf{h}(Y_2|Y_1, X_1) - \mathsf{h}(W_1, W_2) - \mathsf{h}(Y_1|X_1) + \mathsf{h}(Y_1|U' \\ &= \mathsf{h}(Y_2|Y_1, X_1) + \mathsf{h}(Y_1|U', X_1) - \mathsf{h}(W_1, W_2) \\ &\geq \mathsf{h}(Y_2|Y_1, X_1, \mathbf{X}) + \mathsf{h}(Y_1|U', X_1, \mathbf{X}) - \mathsf{h}(W_1, W_2) \\ &= \mathsf{h}(W_2) + \mathsf{h}(W_1) - \mathsf{h}(W_1, W_2) \\ &= 0, \end{aligned} \tag{A.4}$$

which means that $I(\mathbf{X}; Y_1, Y_2|X_1) \geq I(U'; Y_1|X_1)$. So, (A.3) becomes

$$R_1 < I(U'; Y_1|X_1). \tag{A.5}$$

Next, I consider $I(U'; Y_1|X_1)$ where

$$I(U'; Y_1|X_1) = \mathsf{h}(Y_1|X_1) - \mathsf{h}(Y_1|U', X_1) \tag{A.6}$$

The techniques used in the following are quite similar to the ones to deal with $I(U; Y_1|X_1)$ in the paper [30], but it gets a little more complicated due to the vector nature of the transmitted signal and the involvement of the channel coefficients.

For the second item in (A.6), there is

$$\begin{aligned} \mathsf{h}\left(Y_1|U', X_1\right) &\leq \mathsf{h}\left(Y_1\right) \\ &= \mathsf{h}\left(\mathbf{h}_1\mathbf{X} + W_1\right) \\ &\leq \log\left(\pi e \mathbf{h}_1 \mathbf{Q}_{\mathbf{X}} \mathbf{h}_1^H + \pi e N_0\right) \end{aligned} \tag{A.7}$$

and

$$\begin{aligned} \mathsf{h}\left(Y_1|U', X_1\right) &\geq \mathsf{h}\left(Y_1|U', X_1, \mathbf{X}\right) \\ &= \mathsf{h}\left(W_1\right) \\ &= \log\left(\pi e N_0\right) \end{aligned} \tag{A.8}$$

Combining (A.7) and (A.8), it is established that there exists $\alpha \in [0, 1]$ such that

$$\mathsf{h}\left(Y_1|U', X_1\right) = \log\left(\pi e \alpha \mathbf{h}_1 \mathbf{Q}_{\mathbf{X}} \mathbf{h}_1^H + \pi e N_0\right) \tag{A.9}$$

For the first item in (A.6), there is

$$\begin{aligned} \mathsf{h}\left(Y_1|X_1\right) &\geq \mathsf{h}\left(Y_1|U', X_1\right) \\ &= \log\left(\pi e \alpha \mathbf{h}_1 \mathbf{Q}_{\mathbf{X}} \mathbf{h}_1^H + \pi e N_0\right) \end{aligned} \tag{A.10}$$

Also,

$$\begin{aligned} \mathsf{h}\left(Y_1|X_1\right) &= \mathsf{h}\left(\mathbf{h}_1\mathbf{X} + W_1|X_1\right) \\ &\leq \log\left(\pi e \mathsf{Var}\left(\mathbf{h}_1\mathbf{X} + W_1|X_1\right)\right) \\ &= \log\left(\pi e \mathsf{Var}\left(\mathbf{h}_1\mathbf{X}|X_1\right) + \pi e N_0\right) \\ &= \log\left(\pi e \left[\mathsf{E}\left(|\mathbf{h}_1\mathbf{X}|^2\right) - \mathsf{E}\left(|\mathsf{E}\left(\mathbf{h}_1\mathbf{X}|X_1\right)|^2\right)\right] + \pi e N_0\right) \\ &= \log\left(\pi e \left[\mathbf{h}_1 \mathbf{Q}_{\mathbf{X}} \mathbf{h}_1^H - \mathbf{h}_1 \mathsf{E}_{X_1}\left(\mathsf{E}\left(\mathbf{X}|X_1\right)\mathsf{E}\left(\mathbf{X}|X_1\right)^H\right)\mathbf{h}_1^H\right] + \pi e N_0\right) \\ &= \log\left(\pi e \left[\mathbf{h}_1 \mathbf{Q}_{\mathbf{X}} \mathbf{h}_1^H - \mathbf{h}_1 \mathbf{Q}_{\mathsf{E}(\mathbf{X}|X_1)} \mathbf{h}_1^H\right] + \pi e N_0\right), \end{aligned} \tag{A.11}$$

where $\mathsf{E}\left(\mathsf{E}\left(\mathbf{X}|X_1\right)\mathsf{E}\left(\mathbf{X}|X_1\right)^H\right)$ is the auto correlation matrix of the random vector $\mathsf{E}\left(\mathbf{X}|X_1\right)$ and thus, according to the notation definition given before, can be notated as $\mathbf{Q}_{\mathsf{E}(\mathbf{X}|X_1)}$.

From (A.10) and (A.11), I have

$$\mathbf{h}_1 \mathbf{Q}_{\mathbf{X}} \mathbf{h}_1^H - \mathbf{h}_1 \mathbf{Q}_{\mathsf{E}(\mathbf{X}|X_1)} \mathbf{h}_1^H \geq \alpha \mathbf{h}_1 \mathbf{Q}_{\mathbf{X}} \mathbf{h}_1^H, \tag{A.12}$$

and thus

$$\bar{\alpha}\mathbf{h}_1\mathbf{Q}_{\mathbf{X}}\mathbf{h}_1^H \geq \mathbf{h}_1\mathbf{Q}_{\mathsf{E}(\mathbf{X}|X_1)}\mathbf{h}_1^H \overset{(d)}{\geq} 0, \tag{A.13}$$

where (d) is obvious since $\mathbf{h}_1\mathbf{Q}_{\mathsf{E}(\mathbf{X}|X_1)}\mathbf{h}_1^H = \mathsf{E}_{X_1}\left(|\mathsf{E}\left(\mathbf{h}_1\mathbf{X}|X_1\right)|^2\right)$. So, there exists $\bar{\varphi} \in [0,1]$ such that

$$\mathbf{h}_1\mathbf{Q}_{\mathsf{E}(\mathbf{X}|X_1)}\mathbf{h}_1^H = \bar{\varphi}\bar{\alpha}\mathbf{h}_1\mathbf{Q}_{\mathbf{X}}\mathbf{h}_1^H, \tag{A.14}$$

which leads to

$$\mathbf{h}_1\left[\mathbf{Q}_{\mathsf{E}(\mathbf{X}|X_1)} - \bar{\varphi}\bar{\alpha}\mathbf{Q}_{\mathbf{X}}\right]\mathbf{h}_1^H = 0. \tag{A.15}$$

Since (A.15) is true for any given $\mathbf{h}_1$, it follows that

$$\mathbf{Q}_{\mathsf{E}(\mathbf{X}|X_1)} = \bar{\varphi}\bar{\alpha}\mathbf{Q}_{\mathbf{X}}. \tag{A.16}$$

Plugging (A.16) (or (A.14)) into (A.11), I obtain

$$\mathsf{h}\left(Y_1|X_1\right) \leq \log\left(\pi e(\alpha + \bar{\alpha}\varphi)\mathbf{h}_1\mathbf{Q}_{\mathbf{X}}\mathbf{h}_1^H + \pi e N_0\right). \tag{A.17}$$

Then plugging (A.17) and (A.9) into (A.6), I obtain

$$\begin{aligned} I(U';Y_1|X_1) &\leq \log\left(\pi e(\alpha + \bar{\alpha}\varphi)\mathbf{h}_1\mathbf{Q}_{\mathbf{X}}\mathbf{h}_1^H + \pi e N_0\right) - \log\left(\pi e\alpha\mathbf{h}_1\mathbf{Q}_{\mathbf{X}}\mathbf{h}_1^H + \pi e N_0\right) \\ &= \log\left(1 + \frac{\bar{\alpha}\varphi\mathbf{h}_1\mathbf{Q}_{\mathbf{X}}\mathbf{h}_1^H}{\alpha\mathbf{h}_1\mathbf{Q}_{\mathbf{X}}\mathbf{h}_1^H + N_0}\right) \\ &= \mathcal{C}\left(\frac{\bar{\alpha}\varphi\mathbf{h}_1\mathbf{Q}_{\mathbf{X}}\mathbf{h}_1^H}{\alpha\mathbf{h}_1\mathbf{Q}_{\mathbf{X}}\mathbf{h}_1^H + N_0}\right) \end{aligned} \tag{A.18}$$

From (A.5) and (A.18), I obtained

$$R_1 < \mathcal{C}\left(\frac{\bar{\alpha}\varphi\mathbf{h}_1\mathbf{Q}_{\mathbf{X}}\mathbf{h}_1^H}{\alpha\mathbf{h}_1\mathbf{Q}_{\mathbf{X}}\mathbf{h}_1^H + N_0}\right). \tag{A.19}$$

A.2 Proof of outer bound for R_2 in Theorem 1

Let us start with $I(U, X_1; Y_2)$, where

$$I(U, X_1; Y_2) = \mathsf{h}\left(Y_2\right) - \mathsf{h}\left(Y_2|U, X_1\right) \tag{A.20}$$

For the first item in (A.20), there is

$$\begin{aligned}
\mathsf{h}(Y_2) &= \mathsf{h}(\mathbf{h}_2\mathbf{X} + h_3X_1 + W_2) \\
&\leq \log\left(\pi e\left[\mathsf{Var}\left(\mathbf{h}_2\mathbf{X} + h_3X_1\right) + N_0\right]\right) \\
&\leq \log\left(\pi e\left[\begin{array}{cc}\mathbf{h}_2 & h_3\end{array}\right]\left[\begin{array}{cc}\mathbf{Q}_\mathbf{X} & \mathbf{q}_{\mathbf{X}X_1} \\ \mathbf{q}_{\mathbf{X}X_1}^H & P_1\end{array}\right]\left[\begin{array}{c}\mathbf{h}_2^H \\ h_3^*\end{array}\right] + \pi eN_0\right) \\
&= \log\left(\pi e\widetilde{\mathbf{h}}_2\widetilde{\mathbf{Q}}\widetilde{\mathbf{h}}_2^H + \pi eN_0\right)
\end{aligned} \tag{A.21}$$

where $\widetilde{\mathbf{h}}_2 = [\ \mathbf{h}_2 \quad h_3\ ]$ and $\widetilde{\mathbf{Q}} = \left[\begin{array}{cc}\mathbf{Q}_\mathbf{X} & \mathbf{q}_{\mathbf{X}X_1} \\ \mathbf{q}_{\mathbf{X}X_1}^H & P_1\end{array}\right]$. It is obvious that $\widetilde{\mathbf{Q}}$ is the correlation matrix of $[\mathbf{X}^T, X_1]^T$.

For the second item in (A.20), there is

$$\begin{aligned}
\mathsf{h}(Y_2|U, X_1) &\geq \mathsf{h}(Y_2|U, X_1, \mathbf{X}) \\
&= \mathsf{h}(W_2) = \log(\pi eN_0).
\end{aligned} \tag{A.22}$$

Remark: During my derivation, I found that I could introduce $\xi \in [0, 1]$ and give a tighter expression $\mathsf{h}(Y_2|U, X_1) \geq \log\left(\pi e\xi(1 - \bar{\varphi}\bar{\alpha})\mathbf{h}_2\mathbf{Q}_\mathbf{X}\mathbf{h}_2^H + \pi eN_0\right)$. However, since ξ is not used by any other items in the bounds, to obtain the union of the complete bound over ξ is the same to minimize $\mathsf{h}(Y_2|U, X_1)$ over ξ, and I have $\xi = 0$ and $\mathsf{h}(Y_2|U, X_1) \geq \log(\pi eN_0)$, which can actually be obtained via a simpler argument as shown in (A.22).

Plugging (A.21) and (A.22) into (A.20), I obtain

$$\begin{aligned}
I(U, X_1; Y_2) &\leq \log\left(\pi e\widetilde{\mathbf{h}}_2\widetilde{\mathbf{Q}}\widetilde{\mathbf{h}}_2^H + \pi eN_0\right) - \log(\pi eN_0) \\
&= \mathcal{C}\left(\frac{\widetilde{\mathbf{h}}_2\widetilde{\mathbf{Q}}\widetilde{\mathbf{h}}_2^H}{N_0}\right)
\end{aligned} \tag{A.23}$$

Since $\mathbf{q}_{\mathbf{X}X1}$ has nothing to do with R_1, the expression above for R_2 can be maximized over valid $\mathbf{q}_{\mathbf{X}X1}$. Let $q_{\mathbf{X}X_1,i}$ be the i-th element of $\mathbf{q}_{\mathbf{X}X_1}$. Then

$$\begin{aligned}
|q_{\mathbf{X}X_1,i}|^2 &= |\mathsf{E}\left(X^{(i)}X_1^*\right)|^2 = |\mathsf{E}\left(X_1^*\mathsf{E}\left(X^{(i)}|X_1^*\right)\right)|^2 \\
&\leq \mathsf{E}\left(|X_1|^2\right)\mathsf{E}\left(|\mathsf{E}\left(X^{(i)}|X_1^*\right)|^2\right) \\
&\leq P_1[\mathbf{Q}_{\mathsf{E}(\mathbf{X}|X_1)}]_{i,i}
\end{aligned} \tag{A.24}$$

where $[\mathbf{Q}_{\mathsf{E}(\mathbf{X}|X_1)}]_{i,i}$ is the i-th diagonal element of $\mathbf{Q}_{\mathsf{E}(\mathbf{X}|X_1)}$. Plugging (A.16) into the expression above, I have

$$|q_{\mathbf{X}X_1,i}|^2 \leq \bar{\varphi}\bar{\alpha}P_1[\mathbf{Q}_{\mathbf{X}}]_{i,i}, \tag{A.25}$$

or in the vector form

$$|\mathbf{q}_{\mathbf{X}X_1}|^2 \leq \bar{\varphi}\bar{\alpha}P_1\mathsf{diag}\left(\mathbf{Q}_{\mathbf{X}}\right), \tag{A.26}$$

where $\mathsf{diag}\left(\mathbf{Q}_{\mathbf{X}}\right)$ is the vector composed of all diagonal elements of $\mathbf{Q}_{\mathbf{X}}$.

Using (A.26), I can maximize the expression in (A.23) and obtain

$$I(U, X_1; Y_2) \leq \max_{\mathbf{q}_{\mathbf{X}X_1}:|\mathbf{q}_{\mathbf{X}X_1}|^2 \leq \bar{\varphi}\bar{\alpha}P_1\mathsf{diag}(\mathbf{Q}_{\mathbf{X}})} \mathcal{C}\left(\frac{\widetilde{\mathbf{h}}_2\widetilde{\mathbf{Q}}\widetilde{\mathbf{h}}_2^H}{N_0}\right) \tag{A.27}$$

Next, I consider $I(U; Y_1, Y_2|X_1)$ and $I(\mathbf{X}; Y_1, Y_2|U', X_1)$. I obtain

$$\begin{aligned} I(U; Y_1, Y_2|X_1) &= \mathsf{h}\left(Y_1, Y_2|X_1\right) - \mathsf{h}\left(Y_1, Y_2|U, X_1\right) \\ &\leq \mathsf{h}\left(Y_1, Y_2|X_1\right) - \mathsf{h}\left(Y_1, Y_2|U, X_1, \mathbf{X}\right) \\ &= \mathsf{h}\left(Y_1, Y_2|X_1\right) - \mathsf{h}\left(Y_1, Y_2|X_1, \mathbf{X}\right) \\ &= I(\mathbf{X}; Y_1, Y_2|X_1), \end{aligned} \tag{A.28}$$

and

$$I(\mathbf{X}; Y_1, Y_2|U', X_1) \leq I(\mathbf{X}; Y_1, Y_2|X_1) \tag{A.29}$$

where the same arguments as those for $I(\mathbf{X}; Y_1, Y_2|U, X_1)$ in (A.2) are used, since it is obvious that U and U' are reciprocal.

Since

$$\begin{aligned} I(\mathbf{X}; Y_1, Y_2|X_1) &= I(\mathbf{X}; \mathbf{h}_1\mathbf{X} + W_1, \mathbf{h}_2\mathbf{X} + h_3X_1 + W_2|X_1) \\ &= I(\mathbf{X}; \mathbf{h}_1\mathbf{X} + W_1, \mathbf{h}_2\mathbf{X} + W_2|X_1) \\ &= I(\mathbf{X}; \widetilde{\mathbf{Y}}|X_1) \end{aligned} \tag{A.30}$$

where $\widetilde{\mathbf{Y}} = \begin{bmatrix} \mathbf{h}_1 \\ \mathbf{h}_2 \end{bmatrix} \mathbf{X} + \begin{bmatrix} W_1 \\ \mathbf{h}_2 \end{bmatrix}$ and $I(\mathbf{X}; \widetilde{\mathbf{Y}}|X_1)$ stands for the mutual information, conditioned on X_1, of a 2×2 MIMO system with channel matrix $\widetilde{\mathbf{H}} = \begin{bmatrix} \mathbf{h}_1 \\ \mathbf{h}_2 \end{bmatrix}$. I can

obtain $I(\mathbf{X}; Y_1, Y_2|X_1)$ in similar ways to calculate unconditional MIMO capacity by applying singular value decomposition (SVD) to $\widetilde{\mathbf{H}}$.

Let $\widetilde{\mathbf{H}} = \mathbf{U}_{\widetilde{\mathbf{H}}}\mathbf{\Sigma}_{\widetilde{\mathbf{H}}}\mathbf{V}_{\widetilde{\mathbf{H}}}^H$ be the SVD of $\widetilde{\mathbf{H}}$ where $\mathbf{\Sigma}_{\widetilde{\mathbf{H}}}$ is a diagonal matrix with σ_i being the i-th diagonal element, then transmission from $\mathbf{X}$ to $\widetilde{\mathbf{Y}}$ is equivalent to transmission over a number of parallel channels (2 parallel channels in my case) as

$$\left(\mathbf{U}_{\widetilde{\mathbf{H}}}^H\widetilde{\mathbf{Y}}\right)_i = \sigma_i\left(\mathbf{V}_{\widetilde{\mathbf{H}}}^H\mathbf{X}\right)_i + w_i, (i = 1, 2), \tag{A.31}$$

where $(\cdot)_i$ is the i-th entry of the specified vector. It is easy to obtain that w_i $(i = 1, 2)$ is still i.i.d. $\mathcal{CN}(0, N_0)$. For maximal mutual information, $\mathbf{V}_{\widetilde{\mathbf{H}}}^H\mathbf{X}$ needs to have independent entries, which means its correlation matrix $\mathbf{Q}_{\mathbf{V}_{\widetilde{\mathbf{H}}}^H\mathbf{X}} = \mathbf{V}_{\widetilde{\mathbf{H}}}^H\mathbf{Q}_{\mathbf{X}}\mathbf{V}_{\widetilde{\mathbf{H}}}$ is diagonal. Let $\tilde{P}_i$ be its i-th diagonal element, then

$$\mathbf{Q}_{\mathbf{V}_{\widetilde{\mathbf{H}}}^H\mathbf{X}} = \mathbf{V}_{\widetilde{\mathbf{H}}}^H\mathbf{Q}_{\mathbf{X}}\mathbf{V}_{\widetilde{\mathbf{H}}} = \mathsf{diag}(\tilde{P}_1, \tilde{P}_2). \tag{A.32}$$

Also, let $\mathbf{Q}_{\mathsf{E}\left(\mathbf{V}_{\widetilde{\mathbf{H}}}^H\mathbf{X}|X_1\right)}$ be the correlation matrix of $\mathsf{E}\left(\mathbf{V}_{\widetilde{\mathbf{H}}}^H\mathbf{X}|X_1\right)$, then

$$\begin{aligned}
\mathbf{Q}_{\mathsf{E}\left(\mathbf{V}_{\widetilde{\mathbf{H}}}^H\mathbf{X}|X_1\right)} &= \mathsf{E}\left(\mathsf{E}\left(\mathbf{V}_{\widetilde{\mathbf{H}}}^H\mathbf{X}|X_1\right)\mathsf{E}\left(\mathbf{V}_{\widetilde{\mathbf{H}}}^H\mathbf{X}|X_1\right)^H\right) \\
&= \mathbf{V}_{\widetilde{\mathbf{H}}}^H\mathsf{E}\left(\mathsf{E}\left(\mathbf{X}|X_1\right)\mathsf{E}\left(\mathbf{X}|X_1\right)^H\right)\mathbf{V}_{\widetilde{\mathbf{H}}} \\
&= \mathbf{V}_{\widetilde{\mathbf{H}}}^H\mathbf{Q}_{\mathsf{E}(\mathbf{X}|X_1)}\mathbf{V}_{\widetilde{\mathbf{H}}} \\
&\overset{(2b)}{=} \bar{\varphi}\bar{\alpha}\mathbf{V}_{\widetilde{\mathbf{H}}}^H\mathbf{Q}_{\mathbf{X}}\mathbf{V}_{\widetilde{\mathbf{H}}} \\
&\overset{(2c)}{=} \bar{\varphi}\bar{\alpha}\mathsf{diag}(\tilde{P}_1, \tilde{P}_2)
\end{aligned} \tag{A.33}$$

where $(2b)$ is obtained by plugging (A.16) and $(2c)$ is obtained by plugging (A.32).

So,

$$\begin{aligned}
I(\mathbf{X}; \widetilde{\mathbf{Y}}|X_1) &= \textstyle\sum_{i=1}^2 I(\left(\mathbf{V}_{\widetilde{\mathbf{H}}}^H\mathbf{X}\right)_i; \left(\mathbf{U}_{\widetilde{\mathbf{H}}}^H\widetilde{\mathbf{Y}}\right)_i|X_1) \\
&\leq \textstyle\sum_{i=1}^2 \log\left(1 + \frac{|\sigma_i|^2(\mathsf{E}\left(|\left(\mathbf{V}_{\widetilde{\mathbf{H}}}^H\mathbf{X}\right)_i|^2\right) - \mathsf{E}\left(|\mathsf{E}\left(\left(\mathbf{V}_{\widetilde{\mathbf{H}}}^H\mathbf{X}\right)_i|X_1\right)|^2\right))}{N_0}\right) \\
&= \textstyle\sum_{i=1}^2 \log\left(1 + \frac{|\sigma_i|^2(\tilde{P}_i - \bar{\varphi}\bar{\alpha}\tilde{P}_i)}{N_0}\right) \\
&= \log\left(\textstyle\prod_{i=1}^2 1 + \frac{(1-\bar{\varphi}\bar{\alpha})|\sigma_i|^2\tilde{P}_i}{N_0}\right) \\
&\overset{(2d)}{=} \log\left(\det\left(\mathbf{I} + \frac{1-\bar{\varphi}\bar{\alpha}}{N_0}\widetilde{\mathbf{H}}\mathbf{Q}_{\mathbf{X}}\widetilde{\mathbf{H}}^H\right)\right)
\end{aligned} \tag{A.34}$$

where $(2d)$ follows from the fact that $1 + \frac{(1-\bar{\varphi}\bar{\alpha})|\sigma_i|^2\tilde{P}_i}{N_0}$ is the eigenvalue of $\mathbf{I} + \frac{1-\bar{\varphi}\bar{\alpha}}{N_0}\widetilde{\mathbf{H}}\mathbf{Q}_{\mathbf{X}}\widetilde{\mathbf{H}}^H$.

Appendix B

MMSE Cooperative Positioning

B.1 Derivation for MMSE Cooperative Position Estimator (5.11)

Recalling form the section 5.4.2 that $\boldsymbol{\theta} = (x_1, y_1, \cdots, x_N, y_N)$ stands for all unknown coordinates to be estimated, and $\mathbf{P} = (P_{ij} | 1 \leq i \leq N, i{+}1 \leq j \leq N{+}M)$ represents the collection of power degradations between each pair of N unknown nodes and between each unknown node and the M anchor nodes. A node j, $j = N{+}1, \cdots, N{+}M$ refers to one of the M anchor nodes.

Let $f(\boldsymbol{\theta}|\mathbf{P})$ be the posterior PDF of $\boldsymbol{\theta}$ given the observation $\mathbf{P}$. Then, according to (5.8), there is

$$\begin{aligned} \hat{x}_{i,\text{MMSE}} &= \int_{S_{\boldsymbol{\theta}}} x_i f(\boldsymbol{\theta}|\mathbf{P}) d\boldsymbol{\theta} \\ \hat{y}_{i,\text{MMSE}} &= \int_{S_{\boldsymbol{\theta}}} y_i f(\boldsymbol{\theta}|\mathbf{P}) d\boldsymbol{\theta} \end{aligned}, \tag{B.1}$$

where $\int \cdot d\boldsymbol{\theta}$ is a short hand for multiple integrals with respect to x_1,y_1,...,x_N,y_N and $S_{\boldsymbol{\theta}}$ is the integral region for $\boldsymbol{\theta}$.

Since

$$f(\boldsymbol{\theta}|\mathbf{P}) = \frac{f(\mathbf{P}|\boldsymbol{\theta}) f(\boldsymbol{\theta})}{\int_{S_{\boldsymbol{\theta}}} f(\mathbf{P}|\boldsymbol{\theta}) f(\boldsymbol{\theta}) d\boldsymbol{\theta}}, \tag{B.2}$$

and the a priori PDF has been given in (5.10), we only need the likelihood function $f(\mathbf{P}|\boldsymbol{\theta})$ to compute the posterior PDF $f(\boldsymbol{\theta}|\mathbf{P})$.

The coordinates of the anchor nodes ($j = N{+}1, \cdots, N{+}M$) are known and fixed. Then, given the coordinates of all unknown nodes $\boldsymbol{\theta}$, entries in $\mathbf{P}$ are independent from each other. Thus, we have

$$\begin{aligned} f(\mathbf{P}|\boldsymbol{\theta}) &= \prod_{i=1}^{N} \prod_{j=i+1}^{N+M} f(P_{ij}|\boldsymbol{\theta}) \\ &\overset{(a)}{=} \prod_{i=1}^{N} \prod_{j=i+1}^{N+M} f\left(P_{ij}|(x_i, y_i), (x_j, y_j)\right) \end{aligned}, \tag{B.3}$$

where (a) follows from the fact that P_{ij} is only dependent on the distance between the node i and node j, which can be determined once their coordinates (x_i, y_i) and (x_j, y_j) are given, and thus P_{ij} is independent from the coordinates of other nodes.

From the log-normal distribution for P_{ij} ((5.1) and (5.2)) and the relation $P_{ij}(dB) = 10\log_{10} P_{ij}$, we have

$$\begin{aligned} & f\left(P_{ij}|(x_i,y_i),(x_j,y_j)\right) \\ &= \left|\tfrac{dP_{ij}(dB)}{dP_{ij}}\right| f\left(P_{ij}(dB)|(x_i,y_i),(x_j,y_j)\right) \\ &= \tfrac{10/\ln 10}{P_{ij}} \cdot \tfrac{1}{\sqrt{2\pi\sigma_{dB}^2}} \exp\left[-\tfrac{\left(10\log_{10}\frac{P_{ij}}{P_0}+10n_p\log_{10}\frac{d_{ij}}{d_0}\right)^2}{2\sigma_{dB}^2}\right], \\ &= \tfrac{10/\ln 10}{P_{ij}\sqrt{2\pi\sigma_{dB}^2}} \exp\left[-\tfrac{\alpha}{8}\ln^2\tfrac{d_{ij}^2}{\hat{d}_{ij}^2}\right] \end{aligned} \tag{B.4}$$

where ln is the natural logarithm, and α and $\hat{d}_{ij}$ are expressed in (5.14) and (5.15) respectively. For completeness, they are repeated here

$$\alpha = -\left(\frac{10n_p}{\sigma_{dB}\ln 10}\right)^2,$$

$$\hat{d}_{ij} = d_0\left(\frac{P_0}{P_{ij}}\right)^{1/n_p}.$$

(x_i, y_i) and (x_j, y_j) contribute to the likelihood function via $d_{ij}^2 = (x_i - x_j)^2 + (y_i - y_j)^2$.

Plugging (B.4) into (B.3), we obtain

$$f(\mathbf{P}|\boldsymbol{\theta}) = \prod_{i=1}^{N}\prod_{j=i+1}^{N+M} \frac{10/\ln 10}{P_{ij}\sqrt{2\pi\sigma_{dB}^2}} \exp\left[-\frac{\alpha}{8}\ln^2\frac{d_{ij}^2}{\hat{d}_{ij}^2}\right]. \tag{B.5}$$

Now, we are ready to compute the posterior PDF. Plugging the given a priori PDF (5.10) and the derived likelihood function (B.5) in (B.2), the final expression for $f(\boldsymbol{\theta}|\mathbf{P})$ is

$$f(\boldsymbol{\theta}|\mathbf{P}) = \frac{\prod_{i=1}^{N}\prod_{j=i+1}^{N+M}\exp\left[-\frac{\alpha}{8}\ln^2\frac{d_{ij}^2}{\hat{d}_{ij}^2}\right]}{\int_{S_{\boldsymbol{\theta}}}\prod_{i=1}^{N}\prod_{j=i+1}^{N+M}\exp\left[-\frac{\alpha}{8}\ln^2\frac{d_{ij}^2}{\hat{d}_{ij}^2}\right]d\boldsymbol{\theta}}, \tag{B.6}$$

for $\boldsymbol{\theta} \in S_{\boldsymbol{\theta}}$ where $S_{\boldsymbol{\theta}}$ can be easily obtained as

$$S_{\boldsymbol{\theta}} = \left\{\boldsymbol{\theta}\middle| \begin{array}{l} x_i \in (O_{ix} - A_i, O_{ix} + A_i) \\ y_i \in (O_{iy} - B_i, O_{iy} + B_i) \end{array}, 1 \le i \le N\right\}. \tag{B.7}$$

Plugging (B.6) in (B.1), we obtain the MMSE cooperative position estimator as

$$\begin{aligned}\hat{x}_{i,\text{MMSE}} &= \frac{\int_{S_{\boldsymbol{\theta}}} x_i \prod_{i=1}^{N}\prod_{j=i+1}^{N+M} \exp\left[-\frac{\alpha}{8}\ln^2\frac{d_{ij}^2}{\hat{d}_{ij}^2}\right] d\boldsymbol{\theta}}{\int_{S_{\boldsymbol{\theta}}} \prod_{i=1}^{N}\prod_{j=i+1}^{N+M} \exp\left[-\frac{\alpha}{8}\ln^2\frac{d_{ij}^2}{\hat{d}_{ij}^2}\right] d\boldsymbol{\theta}} \\ \hat{y}_{i,\text{MMSE}} &= \frac{\int_{S_{\boldsymbol{\theta}}} y_i \prod_{i=1}^{N}\prod_{j=i+1}^{N+M} \exp\left[-\frac{\alpha}{8}\ln^2\frac{d_{ij}^2}{\hat{d}_{ij}^2}\right] d\boldsymbol{\theta}}{\int_{S_{\boldsymbol{\theta}}} \prod_{i=1}^{N}\prod_{j=i+1}^{N+M} \exp\left[-\frac{\alpha}{8}\ln^2\frac{d_{ij}^2}{\hat{d}_{ij}^2}\right] d\boldsymbol{\theta}}\end{aligned} \tag{B.8}$$

To emphasize that the definite integrals in (B.8) are multiple integrals, we introduce $\int \cdot\, d\boldsymbol{\theta}_i$ as a shorthand for $\int\int \cdot\, dx_i dy_i$ as given in (5.12) and the integral region for $\boldsymbol{\theta}_i = (x_i, y_i)$ is denoted as S_i as expressed in (5.13), which is repeated here

$$S_i = \left\{ (x_i, y_i) \middle| \begin{array}{l} x_i \in (O_{ix} - A_i, O_{ix} + A_i) \\ y_i \in (O_{iy} - B_i, O_{iy} + B_i) \end{array} \right\}.$$

Then, the final MMSE cooperative position estimator as expressed in (5.11) is obtained.

B.2 Derivation for $\hat{d}_{ij}$ expression (5.16)

From (5.15), we obtain

$$\begin{aligned}10\log_{10}\hat{d}_{ij} &= \frac{1}{n_p} 10\log_{10}\frac{P_0}{P_{ij}} + 10\log_{10} d_0 \\ &= \frac{1}{n_p}(P_0(dB) - P_{ij}(dB)) + 10\log_{10} d_0\end{aligned} \tag{B.9}$$

According to (5.1) and (5.2), there is

$$P_{ij}(dB) \sim \mathcal{N}\left(P_0(dB) - 10n_p log_{10}\left(\frac{d_{ij}}{d_0}\right), \sigma_{dB}^2\right).$$

Then,

$$10\log_{10}\hat{d}_{ij} \sim \mathcal{N}\left(10log_{10}d_{ij}, \frac{\sigma_{dB}^2}{n_p^2}\right).$$

Let G be a standard Gaussian random variable, i.e. $G \sim \mathcal{N}(0,1)$, then

$$\log_{10}\hat{d}_{ij} = log_{10}d_{ij} + \frac{\sigma_{dB}}{10n_p}G,$$

which leads to $\hat{d}_{ij} = d_{ij}10^{\frac{\sigma_{dB}}{10n_p}G}$ (5.16).

BIBLIOGRAPHY

[1] N. Wang and S.D.Blostein, "Comparison of CP-based single carrier and OFDM with power allocation," *IEEE Trans. Commun.*, vol. 53, pp. 391–394, Mar. 2005.

[2] Z. Wang, X. Ma, and G. Giannakis, "OFDM or single-carrier block transmissions?," *IEEE Trans. Commun.*, vol. 52, pp. 380–394, March 2004.

[3] N.Benvenuto and S. Tomasin, "On the comparison between OFDM and single carrier modulation with a DFE using a frequency-domain feedforward filter," *IEEE Trans. Commun.*, vol. 50, pp. 947–955, June 2002.

[4] D. Falconer, S. L. Ariyavisitakul, A. Benyamin-Seeyar, and B. Eidson, "Frequency domain equalization for single-carrier broadband wireless systems," *IEEE Commun. Mag.*, vol. 40, pp. 58–66, Apr. 2002.

[5] S. M. Alamouti, "A simple transmit diversity technique for wireless communications," *IEEE J. Select. Areas Commun.*, vol. 16, pp. 1451–1458, Oct. 1998.

[6] C. D. et al., "Iterative correction of intersymbol interference: Turbo equalization," *Eur. Trans. Telecommun.*, vol. 6, pp. 507–511, Sept. 1995.

[7] R. Koetter, A. C. Singer, and M. Tüchler, "Turbo equalization," *IEEE Signal Processing Magazine*, vol. 21, pp. 67–80, Jan. 2004.

[8] X. Zhu and R. D. Murch, "Layered space-frequency equalization in a single-carrier MIMO system for frequency-selective channels," *IEEE Trans. Wireless Commun.*, vol. 3, pp. 701–708, May 2004.

[9] M. Tüchler, A. Singer, and R. Koetter, "Minimum mean squared error equalization using a priori information," *IEEE Trans. Signal Processing*, vol. 50, pp. 673–683, Mar. 2002.

[10] S. Zhou and G. B. Giannakis, "Single-carrier space-time block-coded transmissions over frequency-selective fading channels," *IEEE Trans. Inform. Theory*, vol. 49, pp. 164–179, Jan. 2003.

[11] X. Wang and H. Poor, "Iterative (turbo) soft interference cancellation and decoding for coded CDMA," *IEEE Trans. Commun.*, vol. 47, pp. 1046–1061, July 1999.

[12] E. der Meulen, "Transmission of information in a T-terminal discrete memoryless channel," *Ph.D. dissertation*, 1968.

[13] E. der Meulen, "Three-terminal communication channels.," *Advances in Applied Probability*, vol. 3, pp. 120–154, Spring 1971.

[14] T. M. Cover, "Capacity theorems for the relay channel," *IEEE Trans. Inf. Theory*, vol. 25, pp. 572–584, Sept. 1979.

[15] M. G. G. Kramer and P. Gupta, "Cooperative strategies and capacity theorems for relay networks," *IEEE Trans. Inf. Theory*, vol. 51, pp. 3037–3063, Sept. 2005.

[16] A. Sendonaris, E. Erkip, and B. Aazhang, "User cooperation diversity-part I: System description," *IEEE Trans. Commun.*, vol. 51, pp. 1927–1938, Nov. 2003.

[17] A. Sendonaris, E. Erkip, and B. Aazhang, "User cooperation diversity-part II: Implementation aspects and performance analysis," *IEEE Trans. Commun.*, vol. 51, pp. 1939–1948, Nov. 2003.

[18] M. Janani, A. Hedayat, T. E. Hunter, and A. Nosratinia, "Coded cooperation in wireless communications: Space-time transmission and iterative decoding," *IEEE Signal Processing*, vol. 52, pp. 362–371, Feb. 2004.

[19] A. Nosratinia, T. E. Hunter, and A. Hedayat, "Cooperative communication in wireless networks," *IEEE Communications Magazine*, pp. 74–80, Oct. 2004.

[20] J. N. Laneman and G. W.Wornell, "Distributed space-time coded protocols for exploiting cooperative diversity in wireless networks," *IEEE Trans. Inf. Theory*, vol. 49, pp. 2415–2425, Oct. 2003.

[21] J. N. Laneman, D. N. C. Tse, and G. W.Wornell, "Cooperative diversity in wireless networks: Efficient protocols and outage behavior," *IEEE Trans. Inf. Theory*, vol. 50, pp. 3062–3080, Dec. 2004.

[22] R. U. Nabar and H. Bölcskei, "Fading relay channels:performance limits and space-time signal design," *IEEE Trans. Inf. Theory*, vol. 22, pp. 1099–1109, Aug. 2004.

[23] M. Yuksel and E. Erkip, "Diversity gains and clustering in wireless relaying," in *IEEE Int. Symp.Inform. Theory (ISIT)*, (Chicago, IL), 2004.

[24] F. Ng, a. M. C. Juite Hwu, and X. Li, "Asynchronous space-time cooperative communications in sensor and robotic networks," in *IEEE Int. Conf. on Mechatronics & Automation (ICMA)*, (Niagara Falls, Canada), July 2005.

[25] T. M. Cover, "Broadcast channels," *IEEE Trans. Inf. Theory*, vol. 18, pp. 2–14, Jan. 1972.

[26] P. P. Bergmans and T. M. Cover, "Cooperative broadcasting," *IEEE Trans. Inf. Theory*, vol. 20, pp. 317–324, May 1974.

[27] T. M. Cover, "Comments on broadcast channels," *IEEE Trans. Inf. Theory*, vol. 44, pp. 2524–2530, Oct. 1998.

[28] T. M. Cover and J. A. Thomas, *Elements of Information Theory*. New York: John Wiley & Sons, Inc., 1991.

[29] Y. Liang and V. V. Veeravalli, "Cooperative relay broadcast channels," in *Int. Conf. on Wireless Networks, Communications and Mobile Computing*, 2005.

[30] Y. Liang and V. V. Veeravalli, "Cooperative relay broadcast channels," *IEEE Trans. Inf. Theory*, vol. 53, pp. 900–928, Mar. 2007.

[31] M. Yuksel and E. Erkip, "Diversity-multiplexing tradeoff in multiple-antenna relay systems," in *In Proceedings of IEEE International Symposium on Information Theory*, (Seattle, WA), pp. 1154–1158, July 2006.

[32] G. Caire and S. Shamai, "On achievable rates in a multi-antenna broadcast downlink," in *38th Annual Allerton Conference on Commun., Control and Computing*, (Monticello, IL), Oct. 2000.

[33] M. H. M. Costa, "Writing on dirty paper," *IEEE Trans. Inf. Theory*, vol. 29, pp. 439 – 441, May 1983.

[34] S. Vishwanath, N. Jindal, and A. Goldsmith, "On the capacity of multiple input multiple output broadcast channels," in *IEEE International Conference on Communications (ICC), 2002*, (Monticello, IL), pp. 1444–1450, May 2002.

[35] P. Viswanath and D. Tse, "Sum capacity of the multiple antenna gaussian broadcast channel and uplink-downlink duality," *IEEE Trans. Inf. Theory*, vol. 49, pp. 1912–1921, Aug. 2003.

[36] L. Zheng and D. Tse, "Diversity and multiplexing: A fundamental tradeoff in multiple-antenna channels.," *IEEE Trans. Inf. Theory*, vol. 49, pp. 1073–1096, May 2003.

[37] D. N. C. Tse, P. Viswanath, and L. Zheng, "Diversity-multiplexing tradeoff in multiple-access channels," *IEEE Trans. Inf. Theory*, vol. 50, pp. 1859–1874, Sept. 2004.

[38] C. Savarese, J. Rabaey, and J. Beutel, "Locationing in distributed ad hoc wireless sensor networks," in *Proc. 2001 Int'l Conf. Acoustics, Speech, and Signal Processing (ICASSP 2001)*, vol. 4, pp. 2037–2040, IEEE, Piscataway, NJ, May 2001.

[39] T. Cox and M. Cox, *Multidimensional Scaling*. Chapman & Hall, London, 1994.

[40] J. A. Costa, N. Patwari, and A. O. Hero III, "Distributed weighted-multidimensional scaling for node localization in sensor networks."

[41] N. Patwari, R. O'Dea, and Y. Wang, "Relative location in wireless networks," (Proc. IEEE VTC 2001).

[42] in *IEEE Standards 802 Part 15.4: Wireless Medium Access Control (MAC) and Physical Layer (PHY) Specifications for Low-Rate Wireless Personal Area Networks (LR-WPANS)*, (IEEE Inc.), 2003.

[43] in *ZigBee Specification v.1.0.*, (ZigBee Alliance), 2005.

[44] S. Tadakamadla, "Indoor local positioning system for zigbee based on rssi," in *M.Sc. Thesis report*, (Department of Information Technology and Media (ITM), Mid Sweden University).

[45] W.-C. Park and M.-H. Yoon, "The implementation of indoor location system to control zigbee home network sice-icase," in *International Joint Conference*, (in Bexco, Busan, Korea), pp. 18–21, Oct. 2006.

[46] T. Rappaport, *Wireless Communications: Principles and Practice*. New Jersy: Prentice-Hall Inc., 1996.

[47] H. Van Trees in *Detection, Estimation, and Modulation Theory, Part I*, (Wiley Inc. New York), 1968.

[48] S. Kay, *Fundamentals of Statistical Signal Processing:Estimation Theory.* New Jersy: Prentice-Hall Inc., 1993.

[49] N. Patwari, A. O. Hero III, M. Perkins, N. S.Correal, and R. J.O'Dea, "Relative location estimation in wireless sensor neworks," *IEEE Transaction on Signal Processing*, vol. 51, pp. 2137–2148, Aug 2003.

[50] A. C. Aitken in *Determinants and Matrices. 4th ed.*, (Edinburgh:Oliver and Boyd), 1946.

[51] P. Groenen in *The majorization approach to multidimensional scaling:some problems and extensions.*, (DSWO Press).

[52] T. F. A. Kitasuka, T. Nakanishi, "Communications, computers and signal processing, 2003. pacrim," pp. 272–275, Aug. 2003.

[53] P. Bahl P, "Radar: an in-building rf-based user location and tracking system,," (Tel-Aviv, Israel,), pp. 775–784, 2000.

[54] J. Pahlavan, K. Xinrong Li Makela, "Indoor geolocation science and technology," *Communications Magazine, IEEE*, vol. 40, no. 2, pp. 112–118, 2002.

[55] E. O. T. Okumura and K. Fukuda, "Field strength and its variability in vhf and uhf land mobile service," *Review Electrical Communication Laboratory*, vol. 16, pp. 494–502, Sep.-Oct. 1968.

[56] M. Hata, "Empirical formula for propagation loss in land mobile radio service," *IEEE Trans. on Veh.Tech.*, vol. 29, pp. 317–325, Aug. 1980.

[57] J. Coulson, A. Williamson, and R. Vaughan, "A statistical basis for lognormal shadowing effects in multipath fading channels.," *IEEE Trans. on Veh.Tech.*, vol. 46, pp. 494–502, April 1998.

[58] A. Goldsmith, *Wireless Communications.* Cambridge University Press., 2005.

[59] G. B. Giannakis in *Ultra-Wideband Communications:An Idea whose Time has Come*, (ICASSP 2003 Plenary Talk), 2003.

[60] D. Webster, "A pulsed ultrasonic distance measurement system based upon phase digitizing," *IEEE Transaction on Instrumentation and Measurement*, vol. 43, no. 4, pp. 578–582, 1994.

[61] H.-L. Song, "Automatic vehicle location in cellular communications systems," *IEEE Transaction on Vehicular Technology*, vol. 43, pp. 902–908, Nov 1994.

[62] Y. Zhao, L. Dong, J. Wang, B. Hu, and Y. Fu, "Implementing indoor positioning system via zigbee devices," (42nd Annual Asilomar Conference on Signals, Systems, and Computers), 2008.

[63] A. O. I. Neal Patwari, "Using proximity and quantized rss for sensor localization in wireless networks," (WSNA 03, San Diego, California, USA), 2003.

[64] N. Patwari, J. N.Ash, S. Kyperountas, A. O.Hero III, R. L. Moses, and N. S. Correal, "Locating the nodes," *IEEE Singal Processing Magazine*, pp. 54–69, July 2005.

[65] N. Patwari, "simMLE," ([online]http://www.eecs.umich.edu/ hero/localize).

[66] W. H. Press, B. P. Flannery, S. A. Teukolsky, and W. T. Vetterling, *Numerical Recipes in C:The Art of Scientific Computing.* Cambridge University Press;2 edition, 1992.

[67] S. Boyd and L. Vandenberghe, *Convex Optimization.* Cambridge: Cambridge University Press, 2004.

[68] D. Fox, J. Hightower, L. Liao, D. Schulz, and G. Borriello, "Bayesian filters for location estimation," (IEEE Pervasive Computing), 2003.

[69] J.-A. Francisco, Y. Chen, E. Elnahraway, K. Kleisouris, and R. P.Martin, "Demo abstract RTBP: Real time Bayesian positioning system for wireless and sensor networks," 2006.

[70] D. Madigan, E. Elnahrawy, R. P.Martin, W.-H. Ju, P. Krishnan, and A. Krishnakuman, "Bayesian indoor positioning systems," (INFOCOM 05), 2005.